iScience

Article

Aberrant mRNA splicing and impaired hippocampal neurogenesis in *Grin2b* mutant mice

Graphical abstract

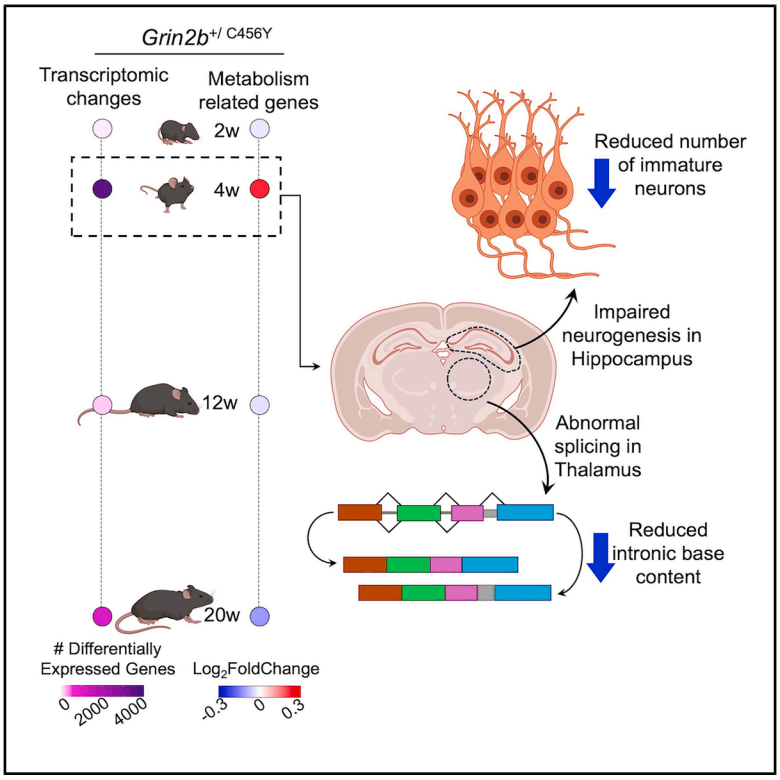

Highlights

- Age-dependent gene expression changes in the brain by ASD-linked *Grin2b*-C456Y mutation
- Alteration of the brain's energy metabolism across ages in *Grin2b*$^{+/C456Y}$ mice
- Abnormal splicing and impaired hippocampal neurogenesis in *Grin2b*$^{+/C456Y}$ mice
- Differential effects of *Grin2b* and *Grin2a* loss-of-function on brain transcriptome

Authors

Zohreh Farsi, Ally Nicolella, Sean K. Simmons, ..., Joshua Z. Levin, Eunjoon Kim, Morgan Sheng

Correspondence

zfarsi@broadinstitute.org

In brief

Molecular biology; Neuroscience; Systems biology

Farsi et al., 2026, iScience *29*, 114700
February 20, 2026
https://doi.org/10.1016/j.isci.2026.114700

CellPress

iScience

CellPress
OPEN ACCESS

Article

Aberrant mRNA splicing and impaired hippocampal neurogenesis in *Grin2b* mutant mice

Zohreh Farsi,[1,6,*] Ally Nicolella,[1] Sean K. Simmons,[1,2] Wangyong Shin,[3] Muwon Kang,[3] Gina Lee,[4] Min Jee Kwon,[1] Kira S. Brenner,[1] Ines Picard,[1] Nate Shepard,[1] Deeksha Misri,[1] Kira A. Perzel Mandell,[1] Joshua Z. Levin,[1,2] Eunjoon Kim,[3,4] and Morgan Sheng[1,5]

[1]Stanley Center for Psychiatric Research, Broad Institute of MIT and Harvard, Cambridge, MA, USA
[2]Klarman Cell Observatory, Broad Institute of MIT and Harvard, Cambridge, MA, USA
[3]Center for Synaptic Brain Dysfunctions, Institute for Basic Science (IBS), Daejeon 34141, Korea
[4]Department of Biological Sciences, Korea Advanced Institute for Science and Technology (KAIST), Daejeon 34141, Korea
[5]Department of Brain and Cognitive Sciences, Massachusetts Institute of Technology, Cambridge, MA, USA
[6]Lead contact
*Correspondence: zfarsi@broadinstitute.org
https://doi.org/10.1016/j.isci.2026.114700

SUMMARY

NMDA receptor dysfunction is implicated in the pathophysiology of autism spectrum disorder (ASD). Here, we investigated heterozygous mouse mutants carrying the ASD-linked C456Y mutation of *Grin2b*, a high-confidence ASD risk gene encoding the GluN2B subunit of NMDA receptors. Comprehensive transcriptomic analyses across brain regions and postnatal ages revealed large-scale gene expression changes, particularly in pathways related to oxidative phosphorylation and ribosome/translation, suggesting brain-wide alteration of energy metabolism and protein synthesis in *Grin2b*$^{+/C456Y}$ mice. We additionally discovered widespread splicing abnormalities and impaired hippocampal neurogenesis in *Grin2b* mutants. Interestingly, the underlying genes and the spatial and temporal patterns of transcriptomic changes in *Grin2b*$^{+/C456Y}$ mice differed substantially from those observed in mutant mice lacking *Grin2a*, encoding the GluN2A subunit of NMDA receptors and a schizophrenia risk gene. These findings underscore the distinct role of *Grin2b* in brain development and function and reveal potential mechanisms by which a lack of *Grin2b* may lead to neurodevelopmental disorders.

INTRODUCTION

Autism spectrum disorder (ASD), with a median prevalence of 1% in the global population,[1] is a neurodevelopmental condition with wide clinical variability. It is characterized by challenges in social interaction and communication, along with repetitive behaviors and restricted interests. The risk of developing ASD has a strong genetic basis; large-scale sequencing studies have identified hundreds of associated genes.[2–14] Despite advances in understanding the complex genetic basis of ASD, its underlying mechanisms remain largely unknown, leaving a significant unmet need for effective therapies. To address this, ASD animal models with human-genetic validity could be beneficial for gaining insights into disease mechanisms and advancing the development of novel therapeutics.

GRIN2B, encoding the GluN2B subunit of the NMDA (N-methyl-*d*-aspartate) receptor (NMDAR), is one of the high-confidence ASD causal genes.[6,13–18] In addition to its strong genetic association, *GRIN2B* is particularly noteworthy in the context of ASD due to its potential for therapeutic intervention. This is supported by the fact that the pharmacological modulation of NMDAR function can potentially alleviate ASD symptoms in humans.[19,20] Furthermore, alterations in NMDAR function are frequently observed in animal models of ASD, even when genes other than those encoding NMDAR subunits are mutated (for example, *Nlgn1*, *Shank2,* and *Shank3*). Restoring NMDAR function in these genetic models has been shown to rescue some ASD-like behaviors.[19–25]

Homozygous deletion of *Grin2b* in mice leads to neonatal death before postnatal day 3.[26] While the synaptic and behavioral effects of brain-wide or cell-specific *Grin2b* homozygous deletion have been previously studied,[27–30] little is known about how a heterozygous mutation affects brain function. This knowledge gap is particularly relevant because in humans with ASD, *GRIN2B* mutations are heterozygous. To gain insights into the role of *Grin2b* in the pathophysiology of ASD, we performed brain-wide analyses of gene expression across multiple developmental stages in a heterozygous knock-in mouse model carrying the ASD-risk mutation GluN2B-C456Y, a *de novo* loss-of-function (LoF) mutation identified in a male individual with ASD and intellectual disability.[16] Previous studies on *Grin2b*$^{+/C456Y}$ mutant mice have demonstrated that the C456Y mutation results in the degradation of the protein product, leading to reduced GluN2B protein level, diminished hippocampal NMDAR currents, and impaired cortical connectivity in *Grin2b*$^{+/C456Y}$ mutant mice.[31,32]

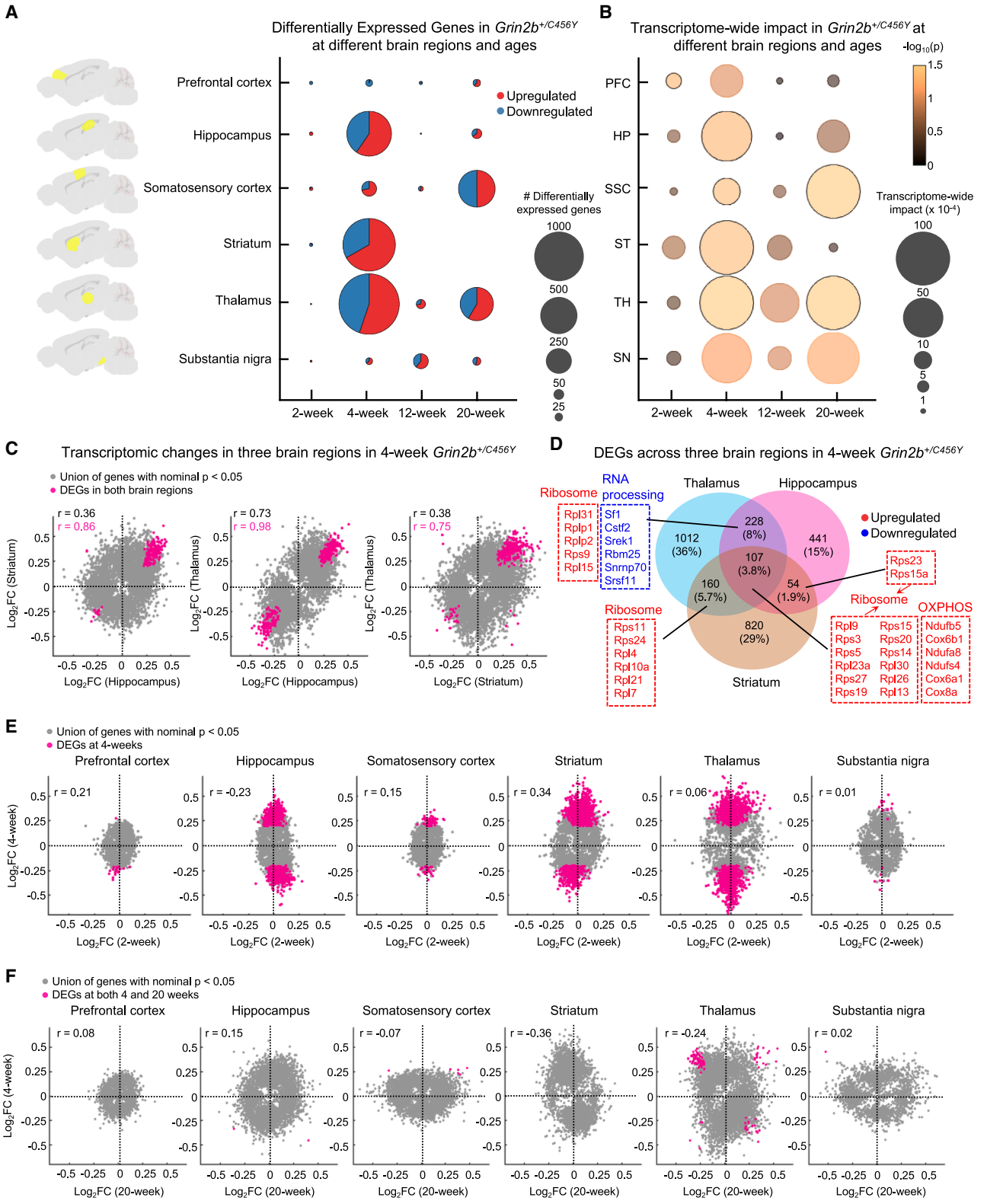

Figure 1. Brain-wide transcriptomic changes in *Grin2b*$^{+/C456Y}$ mice

(A) Number of differentially expressed genes (DEGs; FDR <0.05 and absolute LFC >0.2) in the indicated brain region and age in *Grin2b*$^{+/C456Y}$ mice.

(B) Transcriptome-wide impact in the indicated brain region and age in *Grin2b*$^{+/C456Y}$ mice. Circles with black outlines indicate statistical significance ($p < 0.05$).

(legend continued on next page)

Our comprehensive transcriptomic analysis of *Grin2b*$^{+/C456Y}$ mutants revealed widespread alterations in gene expression in the brain across postnatal development. We identified disruptions in multiple biological processes, including synaptic transmission, RNA processing, translation, chromatin remodeling, neuronal and glial development, and immune function. Similar biological pathways have been implicated in ASD by genetic and postmortem transcriptomic studies in humans.[16,33–41] Of particular interest, we found transcriptomic evidence for disruptions in the brain's energy metabolism, widespread alterations in splicing across multiple brain regions, and reduced hippocampal neurogenesis. Collectively, we identify transcriptomic and other phenotypes that offer insights into the mechanisms by which *Grin2b* LoF contributes to ASD pathophysiology.

RESULTS

Age-dependent effects of *Grin2b* loss-of-function on brain transcriptome

To explore the impact of *Grin2b* heterozygous LoF mutation on the brain, we examined the brain transcriptome of *Grin2b*$^{+/C456Y}$ mutant mice by bulk RNA sequencing (RNA-seq) across six regions—prefrontal cortex (PFC), hippocampus (HP), somatosensory cortex (SSC), striatum (ST), thalamus (TH), and substantia nigra (SN)—at four postnatal ages (2, 4, 12, 20 weeks). The peak transcriptomic effect of *Grin2b-C456Y* mutation, as measured by the number of differentially expressed genes (DEGs, defined as those with a false discovery rate (FDR) < 0.05 and an absolute Log_2Fold Change (LFC) > 0.2) was observed at 4 weeks of age, whereas 2 weeks showed little change and 12 weeks generally showed much fewer DEGs than 4 weeks (Figure 1A; Tables S1 and S2). A similar overall temporal pattern of transcriptomic changes (biggest effects at 4 weeks and 20 weeks) was seen when measured by TRanscriptome-wide Analysis of Differential Expression (TRADE; see STAR Methods and Table S3),[43] which avoids bias from differences in sample size/statistical power between experiments (Figure 1B).

There was no correlation between wild-type *Grin2b* expression levels and the magnitude of transcriptomic effects from *Grin2b-C456Y* mutation across brain regions (Figure S1A). For instance, the thalamus exhibited a large number of DEGs (>1000), despite having relatively low *Grin2b* expression (Figure S1A). By contrast, the PFC showed <100 DEGs, even though *Grin2b* expression is relatively high in this region (Figure S1A). The *Grin2b-C456Y* mutation is associated with reduced GluN1 protein level during the first two weeks of postnatal development.[31] However, mRNA expression of *Grin1* and other NMDAR subunits did not show consistent changes across brain regions and developmental stages in *Grin2b*$^{+/C456Y}$ mice (Figure S1B).

Among the tested brain regions, the hippocampus, striatum, and thalamus exhibited the largest number of DEGs in *Grin2b*$^{+/C456Y}$ mice at 4 weeks, with the majority of these genes being upregulated (Figure 1A). The DEGs in these brain regions showed considerable overlap, with a strong correlation (r = 0.75–0.98) in the LFC of shared DEGs (Figure 1C), suggesting similar gene expression changes across hippocampus, striatum, and thalamus. Interestingly, many genes related to ribosomes, oxidative phosphorylation (OXPHOS), and RNA processing were among these shared DEGs (Figure 1D), and the direction of change of these common DEGs was the same across the three regions.

In line with the lower number of DEGs at 2 and 12 weeks compared to 4 weeks, *Grin2b*$^{+/C456Y}$ mutants showed much larger LFC of individual genes at 4 weeks than at 2 or 12 weeks in most brain regions (Figure 1E; Figure S2A), with modest correlation between 2 and 4 weeks in the striatum (Figure 1E), and between 12 and 4 weeks in the hippocampus (Figure S2A), but little or even inverse correlation in other brain regions. There were a few DEGs shared between the 4-week and 20-week time points (Figures S2B and S2C), and transcriptomic profiles across brain regions displayed little or even inverse correlations between these ages (Figure 1F). This implies that distinct sets of genes are altered at different time points during postnatal development in *Grin2b*$^{+/C456Y}$ mice.

We also tested if there was any overlap between DEGs identified in human ASD samples and differentially regulated genes in *Grin2b*$^{+/C456Y}$ mutants. Indeed, gene set enrichment analysis (GSEA) using DEGs from postmortem cortical tissues of ASD subjects (ages 2–73) in two recent studies[44,45] revealed significant enrichment among differentially regulated genes in *Grin2b*$^{+/C456Y}$ mutants (Figure S3). In particular, genes upregulated in the Gandal et al. study were significantly enriched among upregulated genes across all tested brain regions in 4-week *Grin2b*$^{+/C456Y}$ mice. These results suggest that *Grin2b* LoF can affect similar sets of genes as those altered in human ASD brain tissue.

Perturbation of synapse-, respiration-, and ribosome-related pathways in the brain of *Grin2b*$^{+/C456Y}$ mutants

GSEA revealed that pathways related to synapses/synaptic signaling, chromatin regulation, RNA processing, mRNA translation, OXPHOS, lipid metabolism, and immune response were altered in multiple brain regions, but in an age-dependent fashion (Figure 2A; Table S4). Similar pathways have been found to be dysregulated in gene expression studies of postmortem ASD brain tissues.[35–41] Interestingly, synapse-related pathways showed opposite changes at different developmental stages within the same region. For example, in the thalamus, synapse-related gene sets were enriched among downregulated genes at 4 weeks but among upregulated genes at 20 weeks (hereafter referred to as downregulated or upregulated pathways/Gene Ontology (GO) terms, respectively) (Figure 2A). A negative correlation (r = −0.44) was

(C, E, and F) Gene expression correlation in the indicated brain regions and ages. Pearson's r correlation values are indicated on the plots.
(D) Venn diagram shows the intersection of DEGs from the thalamus, hippocampus, and striatum in 4-week *Grin2b*$^{+/C456Y}$ mice. Genes representative of selected biological pathways of interest are highlighted in the diagram. See Table S1 for the number of samples per brain region, age, and genotype, Table S2 for the full list of DEGs, and Table S3 for TRADE results. Panels A, C-F include the re-analysis of previously published bulk RNA-seq data[42] from the PFC, HP, SSC, ST, and TH of *Grin2b* mutant mice. See also Figures S1–S3 and S8.

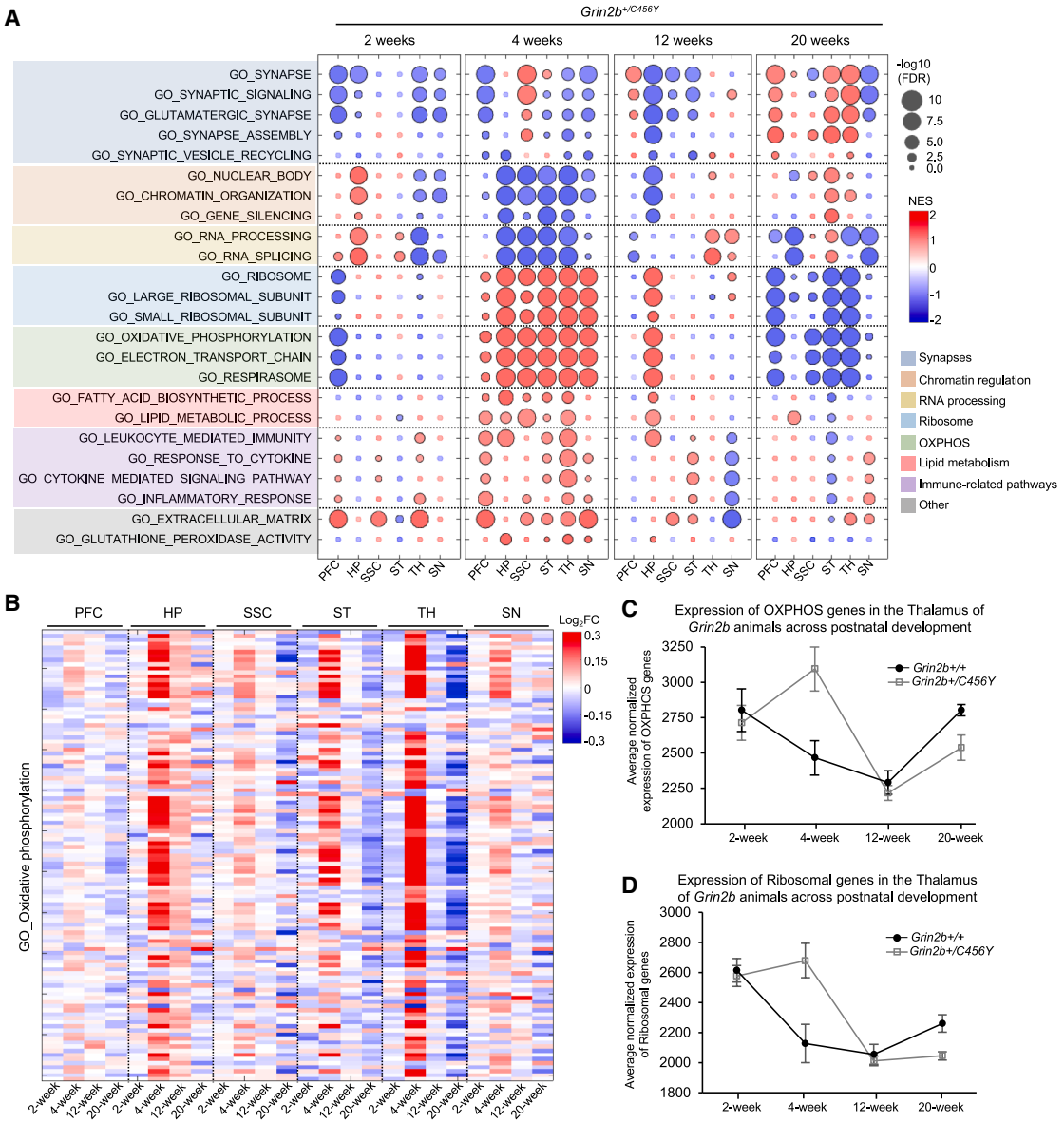

Figure 2. Convergent changes in multiple molecular pathways across six brain regions in *Grin2b*$^{+/C456Y}$ mice

(A) GSEA results for a selection of GO terms from MSigDB that show convergent changes (FDR <0.05) in at least four brain regions in 4-week *Grin2b*$^{+/C456Y}$ mice (see Table S4 for the full list of significantly altered GO terms).

(B) Heatmap shows LFC values for genes within 'GO_Oxidative phosphorylation' term in the studied brain regions of *Grin2b* mutant mice across four postnatal ages.

(C and D) Average DESeq2 normalized expression (see STAR Methods) of oxidative phosphorylation (C), and ribosomal (D) genes in the thalamus of *Grin2b*$^{+/C456Y}$ mice and their wild-type littermates across postnatal development. Data are presented as mean ± standard error of mean (n = 4–5 animals per age and genotype). In (A), circles with black outlines indicate significance (FDR <0.05). This figure includes the re-analysis of previously published bulk RNA-seq data[42] from the PFC, HP, SSC, ST, and TH of *Grin2b* mutant mice. See also Figures S4 and S9.

observed between genes within the GO_Synapse term in the thalamus at these two timepoints (Figure S4A), suggesting that the same genes exhibited opposite changes at 4 and 20 weeks of age.

A similar developmental pattern was observed for pathways related to OXPHOS/mitochondrial respiration and ribosome/translation. These pathways were concordantly upregulated in all tested brain regions in 4-week *Grin2b*$^{+/C456Y}$ mutant mice, but they were downregulated in most brain regions at 20 weeks (Figures 2A and 2B; Figure S4B). Looking into the average expression of OXPHOS and ribosomal genes across the four ages in the thalamus (the brain region with most prominent changes in these pathways), we noted a fall in the expression of these genes from 2 to 4 weeks of age in wild-type mice

(Figures 2C and 2D). In *Grin2b*$^{+/C456Y}$ mice, however, this decrease did not occur at 2 to 4 weeks but was delayed, occurring instead between 4 and 12 weeks (Figures 2C and 2D). This altered temporal pattern of expression of genes related to mitochondrial respiration and translation suggests that the *Grin2b-C456Y* mutation significantly impacts the maturation of brain energy metabolism during early postnatal development.

Brain-wide dysregulation of RNA splicing in *Grin2b*$^{+/C456Y}$ mutants

Gene sets related to RNA processing/splicing were downregulated in most brain regions of 4-week *Grin2b*$^{+/C456Y}$ mutant mice (Figure 2A), raising the possibility of aberrant splicing. We used intron retention analysis of the bulk RNA-seq data (see STAR Methods) to identify genes showing abnormal splicing in *Grin2b*$^{+/C456Y}$ mice as compared to wild types. Specifically, we looked for genes with significantly increased or decreased percent intronic reads (see STAR Methods, and Table S5). In 4-week *Grin2b*$^{+/C456Y}$ mice, the thalamus exhibited the highest number of abnormally spliced genes (defined as those with altered (FDR <0.1) percent intronic reads) (Figure 3A). A similar proportion of the affected genes showed significantly increased or decreased percent intronic reads in the thalamus and hippocampus (Figures 3B and 3C).

Interestingly, multiple glutamate receptor genes, including *Grid1* and *Grid2*, were among the top abnormally spliced genes in the thalamus of 4-week *Grin2b*$^{+/C456Y}$ mice (Figures 3B and 3D). Genes related to fatty acid metabolism, OXPHOS, and synaptic signaling were also observed among shared abnormally spliced genes in the thalamus and the hippocampus (Figure 3D).

By GSEA, pathways related to synapses and neurogenesis/neuron development were enriched among the genes with increased percent intronic reads, while OXPHOS and ribosome-related pathways, as well as RNA processing and immune-related pathways, were enriched among genes with decreased percent intronic reads (Figure 3E). Although we did not specifically measure differential splicing, these findings indicate widespread alterations in splicing efficiency, impacting various molecular pathways across different brain regions in *Grin2b*$^{+/C456Y}$ mice.

In the hippocampus and the thalamus, the two brain regions with the highest number of abnormally spliced genes, we observed reduced expression of many RNA processing-related genes, including those identified as autism risk factors by the Simons Foundation Autism Research Initiative (SFARI) (Figure S5). For instance, *Rbfox1* (also known as *FOX1* or *A2BP1*), a neuron-specific splicing factor and autism susceptibility gene,[46,47] was reduced in the hippocampus, thalamus, and the striatum (FDR <0.1 in all three regions) (Figure 3F). *Rbfox1* is particularly intriguing as a splicing factor, not only due to its genetic association with ASD[48] but also because 41% of its target genes exhibit altered splicing in the brains of humans with ASD.[49] Consistently, *Rbfox1* target genes[50] were significantly enriched among abnormally spliced genes across multiple brain regions in 4-week *Grin2b*$^{+/C456Y}$ mice (Figure 3G), suggesting that the altered expression of *Rbfox1* may contribute to the aberrant splicing observed in *Grin2b*$^{+/C456Y}$ brains. Another notable splicing factor with altered expression in *Grin2b*$^{+/C456Y}$ mutants was *Srrm2* (Figure 3F), whose LoF variants have been linked to schizophrenia and neurodevelopmental disorders.[51,52] Interestingly, haploinsufficiency of *Srrm2* has been shown to cause significant splicing alterations in the mouse brain.[52]

Alteration of different molecular pathways and activity in neuronal cells of *Grin2b*$^{+/C456Y}$ mutants

To explore the cell-type-specific effects of the *Grin2b-C456Y* mutation, we performed single-nucleus RNA-seq (snRNA-seq) of the hippocampus, striatum, and thalamus, the regions with the greatest number of DEGs in 4-week *Grin2b* mutant mice, as well as the PFC, which is known for its role in higher cognitive functions. There were no obvious differences in cell type clustering and proportion between *Grin2b*$^{+/C456Y}$ and wild-type mice in any of the tested brain regions (Figure 4A; Figure S6; Table S6). We performed differential expression analysis of snRNA-seq data using a modified version of pseudocell,[53] a mixed model approach that we used in our previous study[42] (see STAR Methods).

By DEG count (see STAR Methods, and Table S7), neuronal cell types such as pyramidal neurons of layer 2/3 (L2/3IT), and layer 5/6 (L5IT and L6CT) in the PFC, CA1 and CA3 pyramidal cells as well as dentate gyrus (DG) excitatory neurons of the hippocampus, and the inhibitory spiny projection neurons (SPNs) of the striatum showed large transcriptomic changes in 4-week *Grin2b*$^{+/C456Y}$ mutants (Figure 4B). It is important to note that the low number of DEGs in other neuronal cell types may reflect limited statistical power rather than a lack of transcriptomic changes.

By GSEA, distinct as well as common pathways were altered in neuronal cells from various brain regions (Figure 5A; Table S8). In the PFC, pathways related to cell cycle and RNA processing (including genes such as *Srrm2* (a schizophrenia and neurodevelopmental disorder risk gene) and *Hnrnpu* (a high confidence SFARI ASD risk gene)) (Figure 5B)) were downregulated in both the excitatory pyramidal neurons and inhibitory neurons in 4-week *Grin2b*$^{+/C456Y}$ mice (Figure 5A). Conversely, serotonin signaling pathways (including several serotonin receptors (Figure 5C)) were upregulated in multiple neuronal cell types of the PFC (Figure 5A). In the hippocampus, pathways related to synapses, neuron development, and differentiation were significantly downregulated in CA1 pyramidal cells and DG excitatory neurons, while in the striatum and thalamus, ribosome-related pathways showed the most prominent changes across multiple neuronal cells (Figure 5A). These data suggest that the *Grin2b-C456Y* mutation exerts widespread but region-dependent effects on the transcriptome of neuronal cells. In line with this finding, analyzing the correlation between LFC values of nominally significant genes across neuronal cell populations revealed a stronger correlation in transcriptomic changes between neuronal cells within the same brain region, as compared to neurons from distinct brain regions (Figure S7).

Given the significant role of NMDARs in synaptic function, we also assessed the impact of the *Grin2b-C456Y* mutation on neuronal activity by performing GSEA using a curated set of activity-regulated genes (ARGs)[42,54] in neuronal cells. A significant downregulation of ARGs was observed in both excitatory and inhibitory neurons across the tested brain regions, most prominently in the PFC (Figure 5D), implying a brain-wide reduction

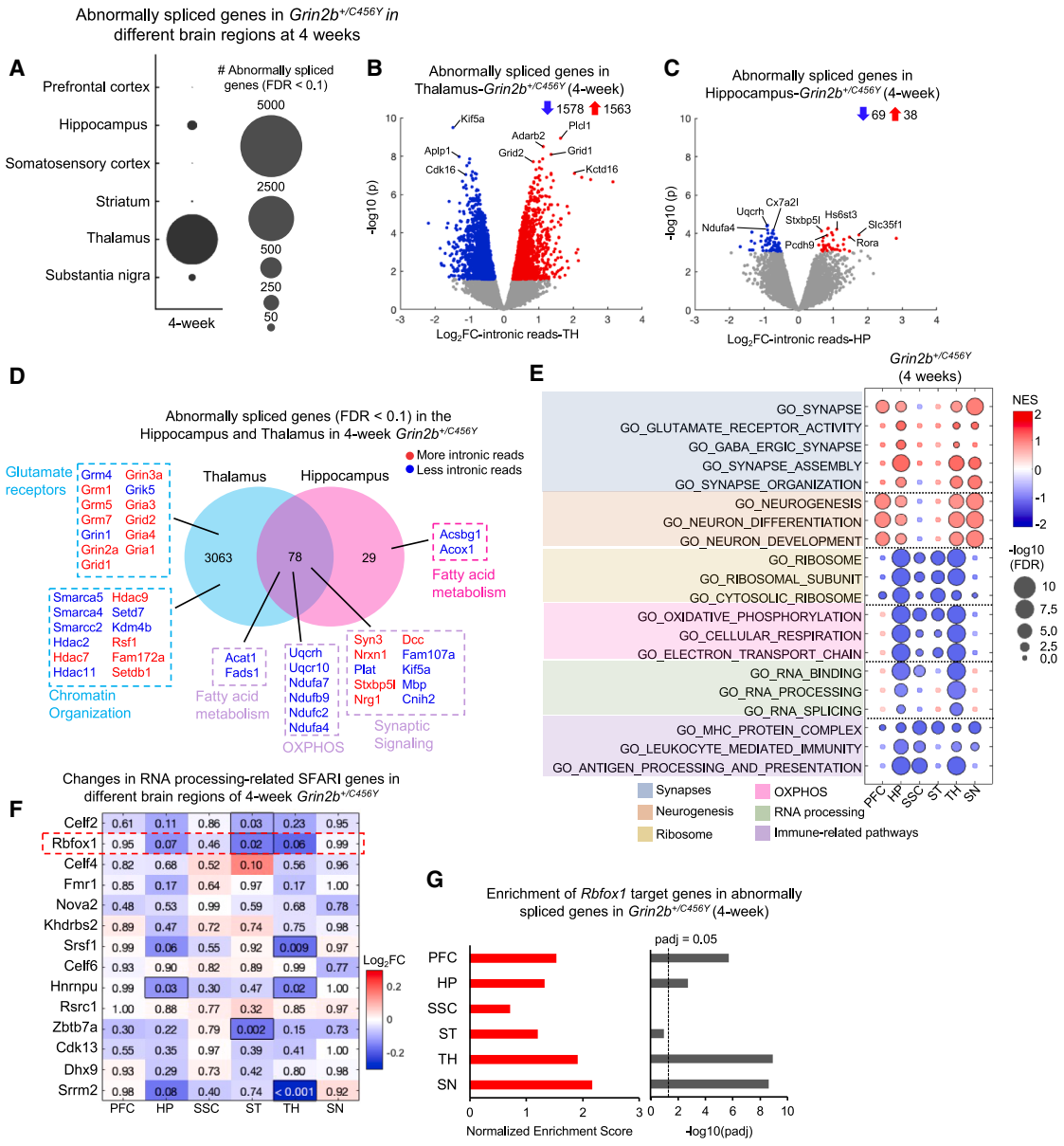

Figure 3. Abnormal splicing in different brain regions in 4-week *Grin2b*$^{+/C456Y}$ mice

(A) Number of abnormally spliced genes (FDR <0.1) in different brain regions of 4-week *Grin2b*$^{+/C456Y}$ mice (see Table S5 for the full list of abnormally spliced genes).

(B and C) Volcano plots show all abnormally spliced genes (blue and red circles represent genes with significantly (FDR <0.1) down- and upregulated percent intronic reads, respectively) in the thalamus (B) and hippocampus (C) in 4-week *Grin2b*$^{+/C456Y}$. Numbers next to blue and red arrows indicate the number of genes with down- and upregulated percent intronic reads, respectively. Top abnormally spliced genes are labeled.

(D) Venn diagram shows the intersection of significantly abnormally spliced genes from the thalamus and hippocampus in 4-week *Grin2b*$^{+/C456Y}$ mice compared to wild types. Genes representative of selected biological pathways of interest are highlighted in the diagram.

(E) GSEA results for a selection of GO terms from MSigDB that show significant enrichment (FDR <0.05) among abnormally spliced genes in at least two brain regions in 4-week *Grin2b*$^{+/C456Y}$ mice.

(F) Heatmap shows the LFC values of RNA processing-related SFARI genes in the bulk RNA-seq data from the tested brain regions in *Grin2b*$^{+/C456Y}$ mice. Numbers indicate FDR values. Black outlines indicate statistical significance (FDR <0.05).

(G) Enrichment of *Rbfox1* target genes among abnormally spliced genes with greater intronic reads in different brain regions of 4-week *Grin2b*$^{+/C456Y}$ mice. In (E), circles with black outlines indicate significance (FDR <0.05). See also Figures S5 and S11.

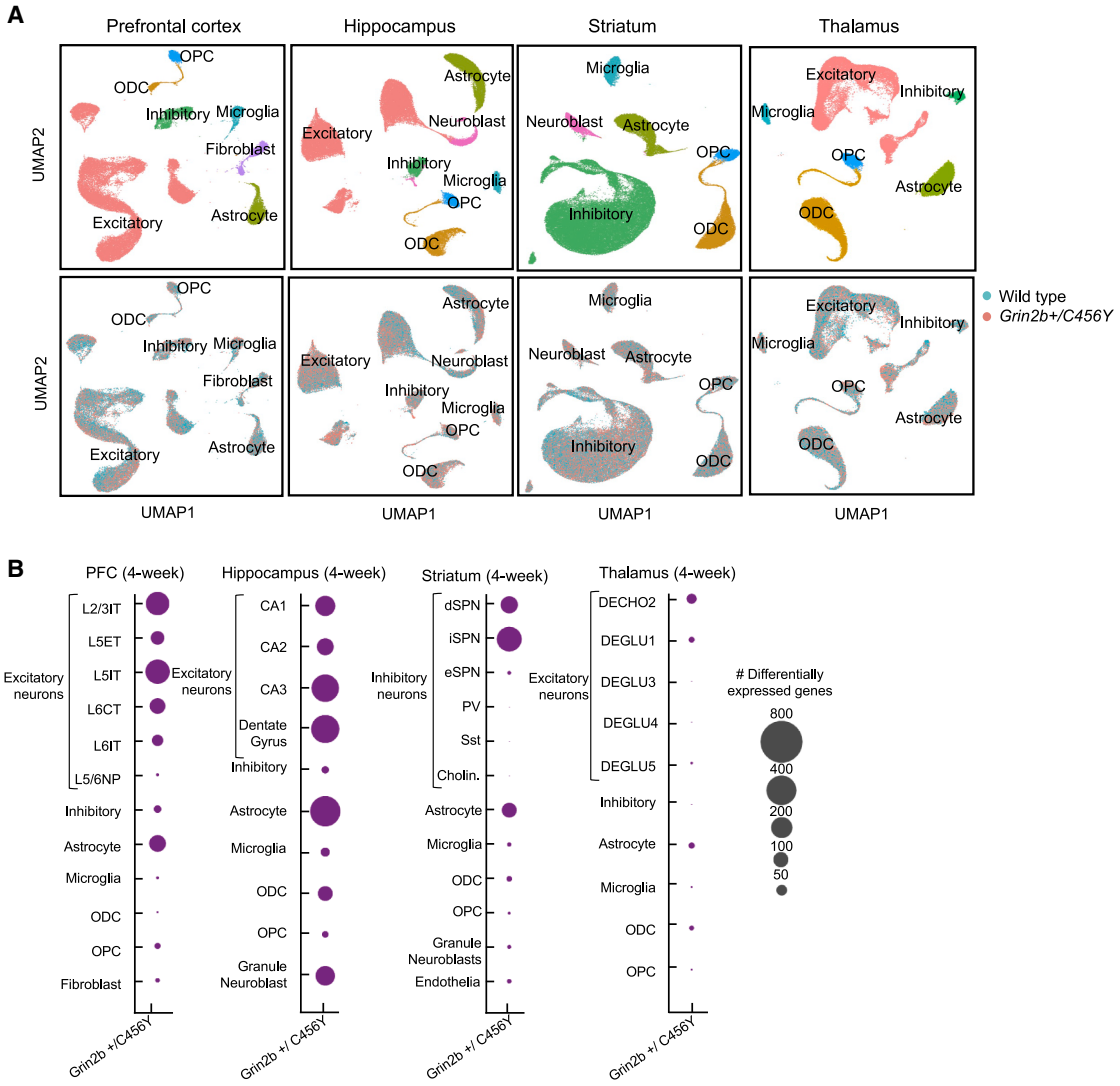

Figure 4. Transcriptomic changes in neuronal and non-neuronal cells in 4-week *Grin2b*$^{+/C456Y}$ mice

(A) UMAP representation of the major cell types identified in the four brain regions studied in the *Grin2b*$^{+/C456Y}$ mouse. Nuclei are colored based on their cell type (upper panel) or their genotype (lower panel).

(B) Number of DEGs across different cell types in the four brain regions studied in the *Grin2b* mutant mouse. ODC, oligodendrocyte; OPC, oligodendrocyte precursor; PV, parvalbumin interneurons; SST, somatostatin interneurons; VIP, vasoactive intestinal peptide interneurons; L2-6 layers; IT, intratelencephalic; NP, near-projecting; ET, extratelencephalic; CT, corticothalamic neuron; dSPN, direct-pathway spiny projection neurons; iSPN, indirect-pathway spiny projection neurons; eSPN, eccentric spiny projection neurons; Cholin., Cholinergic inhibitory neurons. See Table S6 for the number of samples per brain region and genotype, and Table S7 for the full list of DEGs. See also Figure S6.

of neuronal activity in 4-week *Grin2b*$^{+/C456Y}$ mutants. These observations are in line with neuroimaging studies in patients with ASD reporting local hypoconnectivity, particularly in the cortex.[55]

Transcriptomic evidence of altered cholesterol and lipid metabolism in astrocytes and changes in metabolic pathways in glial cells of *Grin2b*$^{+/C456Y}$ mutants

Single nucleus RNA-seq analysis also revealed clear transcriptomic changes in non-neuronal cells in *Grin2b*$^{+/C456Y}$ mice. However, glial cells express low levels of *Grin2b* mRNA (Figure 6A), suggesting that transcriptomic changes in glial cells were potentially driven by the indirect (non-cell-autonomous) effects of *Grin2b* LoF.

Astrocytes, in particular, were affected in *Grin2b*$^{+/C456Y}$ brains, showing a sizable number of DEGs, especially in the hippocampus (Figure 4B; Table S7). We observed limited overlap among DEGs in astrocytes across various brain regions of 4-week *Grin2b*$^{+/C456Y}$ mutants (Figure 6B) which, similar to our observations in neuronal cells, suggests that the effects of *Grin2b-C456Y* mutation on astrocytes depend on the brain region. At the pathway level, a small number of biological

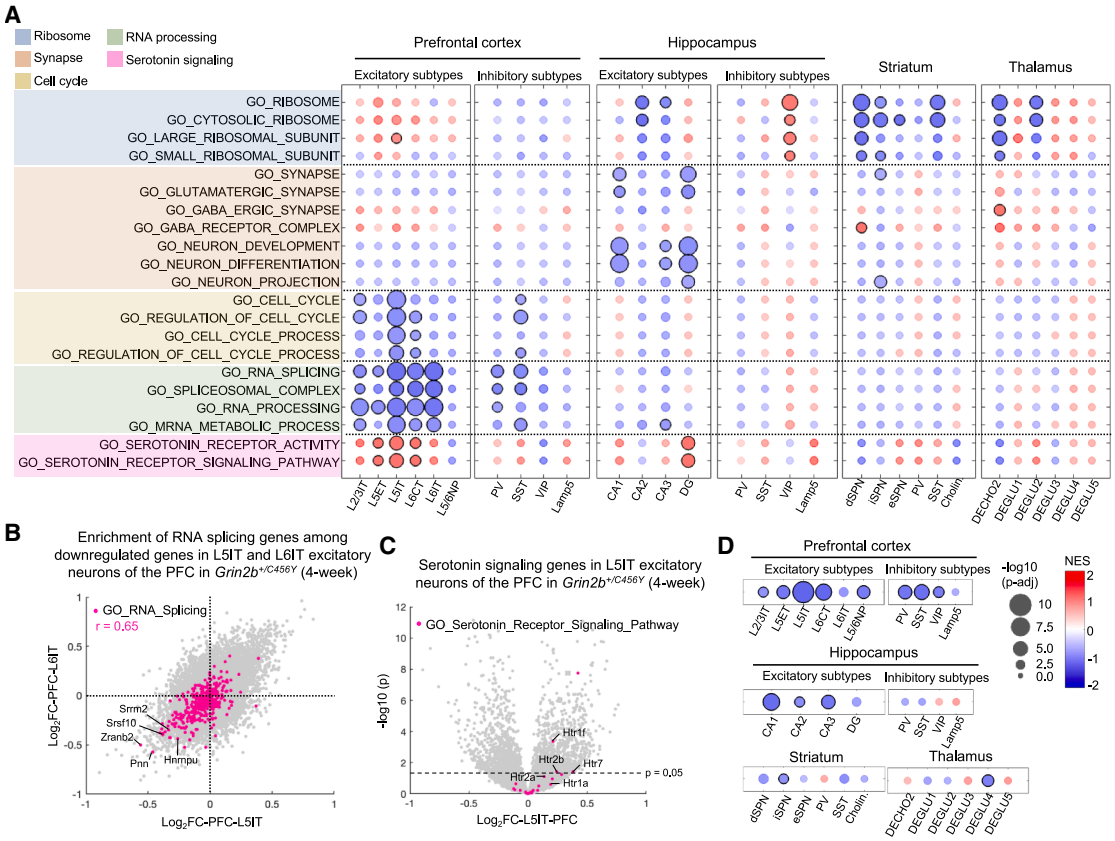

Figure 5. Alteration of various molecular pathways and activity in neuronal cells of different brain regions in 4-week *Grin2b*$^{+/C456Y}$ mice

(A) GSEA results for a selection of GO terms that show changes (FDR <0.05) in neuronal cells in four brain regions of 4-week *Grin2b*$^{+/C456Y}$ mice (See Table S8 for the full list of significantly altered GO terms).

(B) Transcriptomic changes in L5IT versus L6IT excitatory neurons in the PFC of *Grin2b*$^{+/C456Y}$, highlighting the "GO_RNA_splicing" gene set. Pearson's r correlation value for genes within this gene-set is indicated on the plot. Top differentially regulated RNA splicing genes are labeled.

(C) Volcano plot of transcriptomic changes in L5IT excitatory neurons of the PFC, highlighting genes from the indicated GO term. Serotonin receptor genes are labeled.

(D) GSEA results for activity regulated genes in the indicated neuronal populations in *Grin2b*$^{+/C456Y}$ mice. Circles with black outlines indicate statistical significance (p-adj <0.05). See also Figures S7 and S10.

processes were commonly affected in astrocytes across multiple brain regions, and even those exhibited changes in opposite directions in different brain regions (Figure 6C; Table S8). Specifically, pathways associated with steroid metabolism, such as "GO_sterol_metabolic process," which includes *Hmgcr* and *Hmgcs1* (encoding enzymes involved in cholesterol biosynthesis) (Figure 6D), were downregulated in astrocytes of the striatum but upregulated in the PFC. Additionally, lipid metabolism-related pathways such as "GO_lipid_metabolic process" that includes *Acsl6* (involved in fatty acid metabolism), and *Fabp7* (a fatty acid binding protein) (Figure 6E), were upregulated in the astrocytes of the PFC but downregulated in the striatum. However, the expression of individual genes related to steroid and lipid metabolism showed little correlation between astrocytes in the PFC and striatum, suggesting that different genes within these gene sets were altered in the astrocytes of these regions.

OXPHOS and ribosome-related GO terms were significantly and coordinately altered in astrocytes of *Grin2b*$^{+/C456Y}$ mice, though not always in the same direction across brain regions (Figure 6C). Within each brain region, however, the NES score for OXPHOS and ribosomes was highly correlated with each other, and to a lesser extent also with sterol biosynthesis pathways (Figure 6C), suggesting some functional link between these metabolic processes. Besides astrocytes, microglia and oligodendrocytes (ODCs) also exhibited changes in OXPHOS/ribosome-related GO terms (Figure 6F). Overall, the changes in these GO terms in astrocytes were positively correlated with their changes in microglia/ODCs of the same brain region. In line with the bulk RNA-seq results, these data indicate brain-wide alterations in metabolism-related pathways, affecting both neuronal and glial cells in 4-week *Grin2b*$^{+/C456Y}$ mice.

Dysregulation of neurogenesis in the hippocampus of 4-week *Grin2b*$^{+/C456Y}$ mutant mice

In the hippocampus of *Grin2b*$^{+/C456Y}$ mice, granule neuroblasts exhibited a large number of DEGs (Figure 4B). Interestingly, genes related to neurogenesis, such as *Egfr1* (encoding

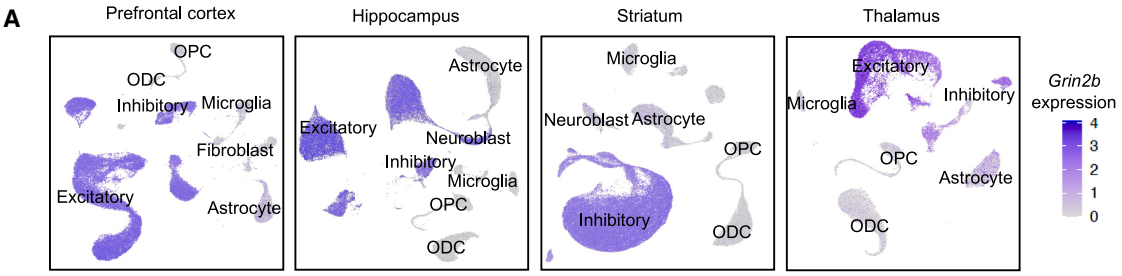

Differentially expressed genes in the Astrocytes of different brain regions in 4-week *Grin2b*$^{+/C456Y}$

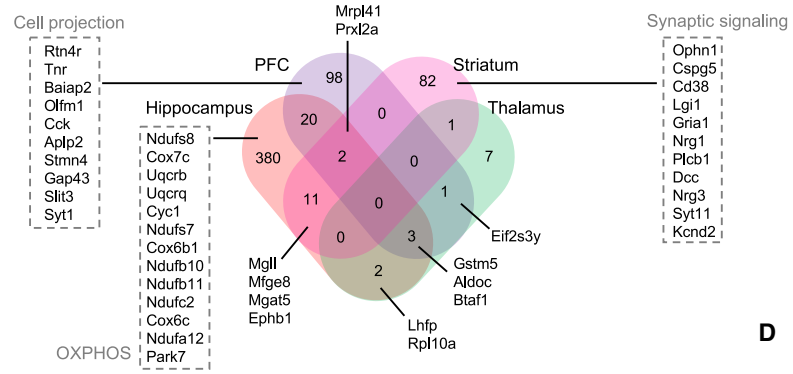

Cholesterol, lipid and metabolism related pathways in the Astrocytes of different brain regions in *Grin2b*$^{+/C456Y}$

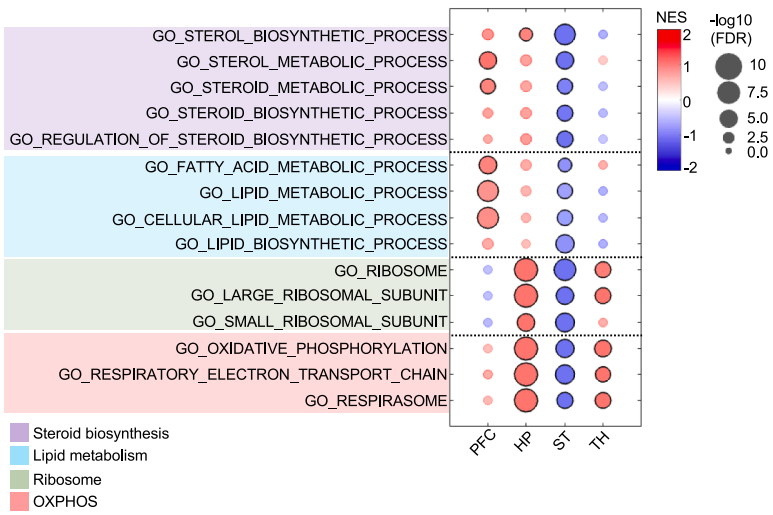

D Cholesterol related genes in astrocytes of the Striatum in *Grin2b*$^{+/C456Y}$ (4-week)

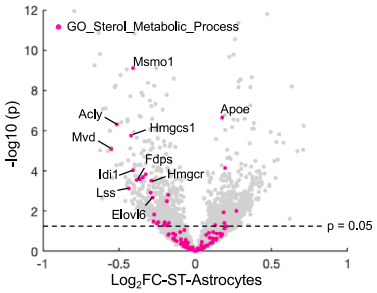

E Lipid metabolism related genes in astrocytes of the PFC in *Grin2b*$^{+/C456Y}$ (4-week)

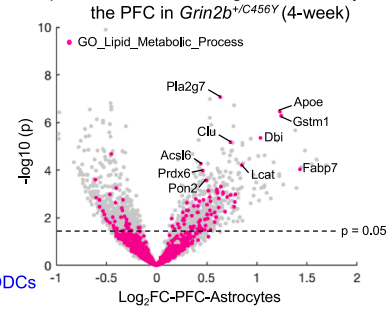

F Metabolism-related pathways in the microglia and ODCs of different brain regions in *Grin2b*$^{+/C456Y}$

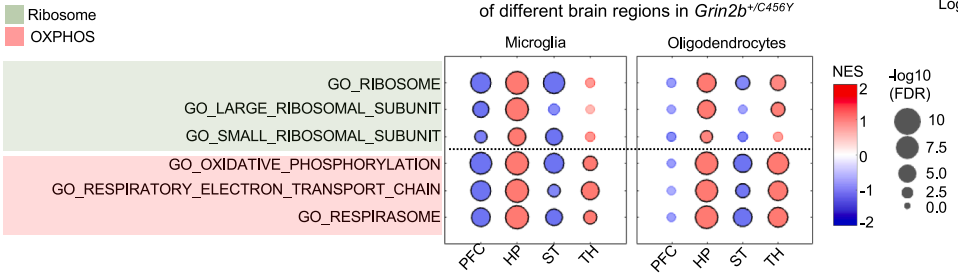

(legend on next page)

epidermal growth factor receptor 1) and *Ephb1* (encoding Ephrin type-B receptor 1), both of which play a role in neuroblast proliferation, were found among downregulated DEGs in 4-week *Grin2b*$^{+/C456Y}$ mice (Figure 7A). Consistent with the DEG findings, GSEA revealed significant downregulation of pathways associated with neurogenesis and neuron development in hippocampal granule neuroblasts of 4-week *Grin2b*$^{+/C456Y}$ mice (Figure 7B). Conversely, pathways related to dopamine, serotonin, and neuropeptide signaling were upregulated in granule neuroblasts (Figure 7B). The decreased expression of neurogenesis-related genes in neuroblasts was accompanied by a significant downregulation of ARGs by GSEA in excitatory neurons of the hippocampus (Figure 5D).

Based on the above findings, we hypothesized that *Grin2b*$^{+/C456Y}$ mice have impaired hippocampal neurogenesis associated with reduced neuronal activity in the hippocampus. To test this hypothesis, we counted the number of immature adult-born neurons in the DG of *Grin2b*$^{+/C456Y}$ mice by labeling for doublecortin (DCX), and observed a significant reduction in DCX^{+} cells in 4-week *Grin2b*$^{+/C456Y}$ mice compared to their wild-type littermates (Figures 7C and 7D). Consistent with this result, we also observed a slight, though not statistically significant, reduction in the number of DCX-expressing granule neuroblasts in our snRNA-seq data. To assess cell proliferation in this brain region, we also performed Ki-67 labeling and found a significant reduction in Ki-67^{+} cells in the hippocampus of *Grin2b*$^{+/C456Y}$ mice (Figures 7C and 7D). Together, these results indicate that the *Grin2b-C456Y* mutation leads to impaired postnatal neurogenesis in the hippocampus, correlated with reduced neuronal activity in this brain region (Figure 5D).

Differential developmental and regional effects of *Grin2a* and *Grin2b* loss-of-function on brain transcriptome

To gain further insights, we compared the brain transcriptomic phenotype of *Grin2b*$^{+/C456Y}$ mutants with that seen in mice with heterozygous LoF of *Grin2a*, a schizophrenia-associated risk gene encoding the GluN2A subunit of NMDARs. In our previous study,[42] we found that transcriptomic changes in the *Grin2a*$^{+/-}$ brain exhibited weak or even inverse correlations with those observed in the same brain regions of *Grin2b*$^{+/C456Y}$ mutants, indicating surprisingly different roles of *Grin2a* and *Grin2b* in brain development and/or function. In the present study, we identified many transcriptomic alterations in *Grin2b*$^{+/C456Y}$ mice that were either absent or different in temporal and/or spatial pattern in *Grin2a*$^{+/-}$ mice. For instance, in contrast to *Grin2b*$^{+/C456Y}$, where the transcriptomic changes were greatest in most brain regions at 4 weeks of age (Figure 1B), *Grin2a*$^{+/-}$ mutants showed a rising transcriptome-wide impact (TWI) that plateaued at 12–20 weeks of age (Figure S8A). Thus, *Grin2a* and *Grin2b* LoF have distinct temporal effects on brain gene expression during development, which is consistent with our previous findings based on the number of DEGs,[42] and potentially explicable by the earlier expression of *Grin2b* than *Grin2a* during development.

One example of a transcriptomic phenotype that is found in *Grin2b*$^{+/C456Y}$ mutants, but different in temporal pattern in *Grin2a*$^{+/-}$ mutants, was the developmental shift in OXPHOS and ribosomal gene expression. Unlike *Grin2b*$^{+/C456Y}$ mutants (see Figures 2B–2D), *Grin2a*$^{+/-}$ mice did not show altered developmental expression of OXPHOS/ribosomal genes compared to their wild-type littermates (Figures S9A–S9D), suggesting that *Grin2a* and *Grin2b* play distinct roles in regulating brain energy metabolism during postnatal development.

Grin2a and *Grin2b* LoF also exert differential brain region effects. In the PFC, *Grin2a*$^{+/-}$ mutants showed significant enrichment of ARGs among downregulated genes across all ages, suggesting persistent PFC hypoactivity in *Grin2a*$^{+/-}$ mice (Figure S8B). By contrast, *Grin2b*$^{+/C456Y}$ mutants exhibited transient downregulation of ARGs in the PFC at 4 weeks, followed by significant upregulation of this gene set by 20 weeks (Figure S8B). In general, *Grin2b*$^{+/C456Y}$ mutants had transcriptomic evidence of increased neuronal activity in most brain regions (except the substantia nigra) at 20 weeks of age. At this age in *Grin2a*$^{+/-}$ mutants, only the hippocampus, and to a lesser extent striatum and thalamus, showed the upregulation of ARGs (Figure S8B).

We previously published that in *Grin2a*$^{+/-}$ mice there was elevated expression of *Drd2* in inhibitory neurons of striatum and a significant upregulation of a dopamine-induced gene set by GSEA.[42] Re-analysis of this snRNA-seq data using the modified pseudocell approach of this current study (see STAR Methods) confirmed significant (padj <0.05) enrichment of dopamine-induced genes among upregulated genes in iSPNs (indirect pathway SPNs) and eccentric SPNs (eSPNs) (Figure S10A); and showed a small but non-significant increase of *Drd2* in pooled inhibitory neurons of the striatum (Figure S10B), which together with other data supports the notion of dysregulated dopamine signaling in the striatum of *Grin2a*$^{+/-}$ mice.[42] To assess whether dopamine signaling might also be dysregulated in *Grin2b*$^{+/C456Y}$ striatum, we examined snRNA-seq data of SPNs. By GSEA, the dopamine-induced gene-set was not significantly altered in any of the inhibitory neuronal subtypes of *Grin2b*$^{+/C456Y}$ striatum (Figure S10C). Thus, unlike *Grin2a*, heterozygous LoF of *Grin2b* is not associated with transcriptomic evidence of a hyperdopaminergic

Figure 6. Changes in metabolism-related pathways in non-neuronal cells of different brain regions in 4-week *Grin2b*$^{+/C456Y}$ mice

(A) UMAP representation of the major cell types identified in the four brain regions studied in the *Grin2b*$^{+/C456Y}$ mice. Nuclei are colored based on *Grin2b* expression.

(B) Venn diagram shows the intersection of DEGs from the astrocytes in four brain regions in 4-week *Grin2b*$^{+/C456Y}$ mutants. Genes representative of selected biological pathways of interest are highlighted in the diagram.

(C and F) GSEA results for a selection of GO terms that show changes (FDR <0.05) in astrocytes (C), microglia, and ODCs (F) in four brain regions of 4-week *Grin2b*$^{+/C456Y}$ mice.

(D and E) Volcano plots of transcriptomic changes in the astrocytes of the striatum (D) and PFC (E), highlighting genes from the indicated GO terms. Top differentially regulated genes within each gene set are labeled.

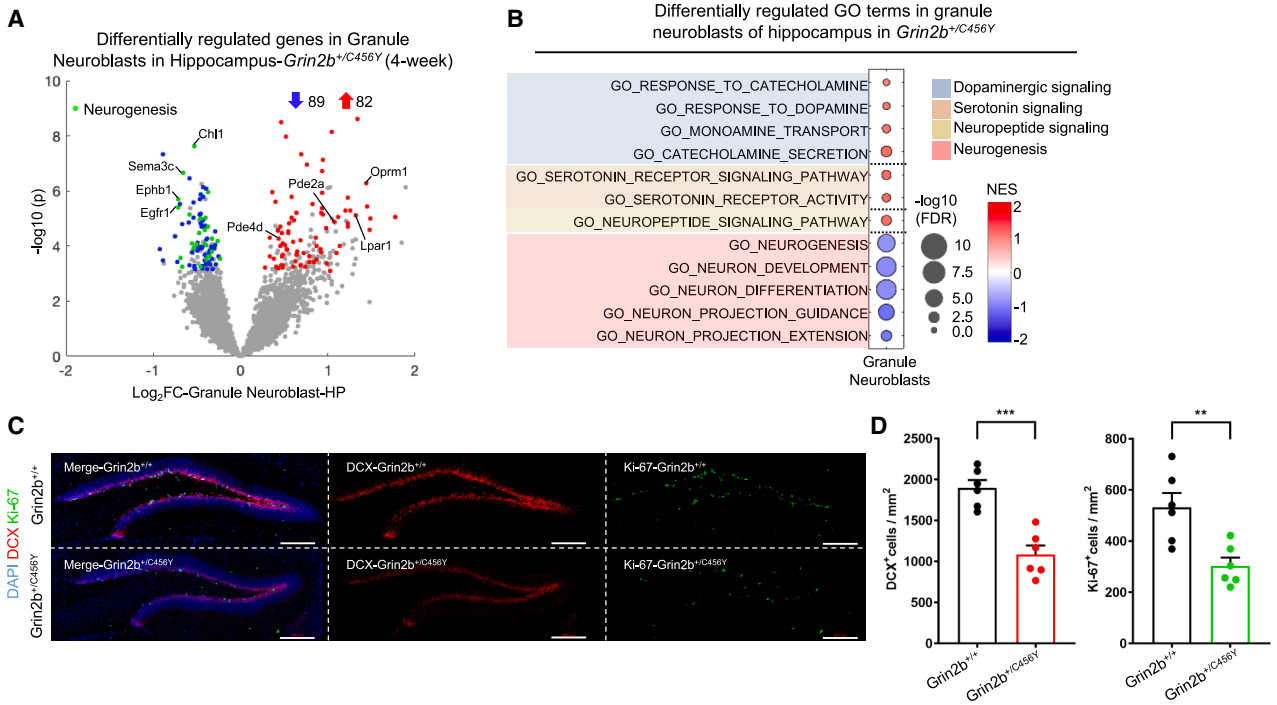

Figure 7. Dysregulation of neurogenesis in the hippocampus of 4-week *Grin2b*$^{+/C456Y}$ mice

(A) Volcano plot shows all significant DEGs (blue and red circles represent down- and upregulated DEGs, respectively) in the granule neuroblasts of the hippocampus in 4-week *Grin2b*$^{+/C456Y}$ mice. Numbers next to blue and red arrows indicate the number of significantly down- and upregulated DEGs, respectively. Genes related to "Neurogenesis" that are found among downregulated DEGs are highlighted in green, and the top ones are labeled. Genes related to "cAMP signaling" that are found among upregulated DEGs are labeled.

(B) GSEA results for a selection of GO terms that show changes (FDR <0.05) in granule neuroblasts of the hippocampus in 4-week *Grin2b*$^{+/C456Y}$ mice.

(C) Representative images of DCX, Ki-67, and DAPI immunostaining in the hippocampal slices of *Grin2b*$^{+/C456Y}$ mice and their wild-type littermates at 4 weeks. Scale bars are 200 μm.

(D) Density of DCX$^+$ and Ki-67$^+$ cells in the hippocampus of *Grin2b*$^{+/C456Y}$ mice and their wild-type littermates at 4 weeks. Two-tailed unpaired Student's *t* test was used to compute *p* values (**$p < 0.01$; ***$p < 0.001$; $n = 6$ per genotype). Data are shown as mean +standard error.

state in the striatum. We note that elevated striatal dopamine signaling does not appear to be a consistent finding in animal models or human studies of ASD.[56]

Another example of region-specific effects of *Grin2b* versus *Grin2a* LoF is in the hippocampus, where granule neuroblasts showed many DEGs and significant downregulation of pathways related to neurogenesis in 4-week *Grin2b*$^{+/C456Y}$ mice (Figure 7). In *Grin2a*$^{+/-}$ mice, by contrast, very few DEGs were observed in hippocampal granule neuroblasts at 4 or 12 weeks,[42] and no transcriptomic evidence of altered hippocampal neurogenesis was observed in these mice. Thus, LoF of *Grin2b,* but not *Grin2a*, seems to impair postnatal hippocampal neurogenesis.

Given the observed aberrant splicing in *Grin2b*$^{+/C456Y}$ mice, we also assessed the effect of *Grin2a* LoF on splicing by performing intron retention analysis at 4 and 12 weeks of age. In 4-week *Grin2a*$^{+/-}$ mice, only a small number of abnormally spliced genes were detected across the six brain regions (Figure S11). At 12 weeks, however, PFC showed the highest number of abnormally spliced genes (Figure S11). This finding is consistent with GSEA results in *Grin2a*$^{+/-}$ mice, where changes in gene sets related to RNA processing/splicing were most prominent in the PFC.[42] Among genes with significantly increased percent intronic reads in PFC (Table S5), pathways related to synaptic signaling, neuronal development, and differentiation were enriched (FDR <0.05). These findings indicate that *Grin2a* haploinsufficiency also disrupts splicing, although with a distinct spatiotemporal profile compared to that observed in *Grin2b*$^{+/C456Y}$ mutants.

DISCUSSION

Our comprehensive gene expression analyses in heterozygous *Grin2b* mutants revealed that the normal decline in the expression of OXPHOS and translation-related genes from 2 to 4 weeks of age no longer occurred in the *Grin2b*$^{+/C456Y}$ mouse brain. This suggests altered respiration and protein synthesis during juvenile brain development in *Grin2b* mutant mice. Impaired energy metabolism and mitochondrial dysfunction have been implicated in ASD pathophysiology and are proposed to be associated with altered neuronal activity.[57] In line with this notion, we found that ARGs, which can serve as surrogate markers of neuronal activity, were significantly enriched among differentially regulated genes across tested brain regions and developmental stages in *Grin2b*$^{+/C456Y}$ mice (Figure S8B). To further explore the relationship between neuronal activity, energy metabolism, and synaptic function, we computed gene set scores for ARGs,

OXPHOS (genes within GO_oxidative_phosphorylation), and synaptic signaling genes (genes within GO_synaptic_signaling) across brain regions and genotypes in 4-week *Grin2b* mice (see Table S9). Scores from all animals and brain regions were pooled by gene set, and pairwise correlations were assessed across gene sets. Notably, ARG and synaptic gene-set scores were highly positively correlated ($r = 0.89$, $p < 0.001$), corroborating a functional interaction between synaptic signaling and activity-regulated genes. On the other hand, an inverse correlation of modest degree was observed between ARG and OXPHOS scores (Spearman's $r = -0.27$, $p = 0.03$), and between synaptic and OXPHOS scores ($r = -0.26$, $p = 0.05$). These findings support the idea that widespread changes in energy metabolism genes may be functionally linked to alterations in neuronal activity and synaptic function in the brain. Because *Grin2b* encodes an excitatory postsynaptic receptor, we hypothesize that the change of brain energy metabolism observed in *Grin2b*$^{+/C456Y}$ mice is likely a downstream consequence of altered neuronal activity resulting from NMDAR dysfunction.

Neuronal activity has also been shown to influence alternative splicing, enabling the dynamic regulation of protein isoform expression in response to external stimuli.[58] The signaling pathways underlying activity-dependent splicing is not well understood; however, calcium/calmodulin-dependent protein kinase IV (CaMKIV)-mediated regulation of RNA-binding proteins has been identified as a major regulator of activity-induced alternative splicing.[59] In this context, the abnormal splicing (as measured here by the inclusion of introns) in the brain of *Grin2b*$^{+/C456Y}$ mice could result from altered CaMKIV activity in response to changes in NMDAR currents[31] and neuronal activity (Figure S8B). Abnormal splicing has been observed in the postmortem brain samples of individuals with ASD, especially in the cortex.[36,39,60–62] Moreover, genes involved in splicing regulation or directly participating in splicing, such as *SRRM2*, *NOVA2*, *WBP4,* and *RBFOX1,* have been associated with ASD,[52,63] underscoring the potential significance of splicing in ASD pathogenesis. A possible mechanism by which aberrant splicing influences ASD pathogenesis is through its effects on neuronal development. Analysis of isoform expression in postmortem brain tissues spanning prenatal and postnatal periods has shown that most expressed genes undergo differential isoform expression during brain development.[64,65] Additionally, *in vitro* corticogenesis has been found to rely substantially on alternative splicing.[65,66] In this context, it is notable that pathways related to synaptic signaling, neuronal development, and differentiation were enriched among abnormally spliced genes across multiple brain regions in *Grin2b*$^{+/C456Y}$ mice (Figure 3E).

We found impaired hippocampal neurogenesis in *Grin2b*$^{+/C456Y}$ mice, based on the following evidence: (i) transcriptomic alterations in granule neuroblasts, including the downregulation of pathways related to neurogenesis, neuron development, and differentiation, (ii) a decrease in the number of newborn neurons (DCX^{+} cells), and (iii) reduced proliferation, as indicated by the lower density of Ki-67^{+} cells in the hippocampus of *Grin2b*$^{+/C456Y}$ mice (Figure 7). Aberrant postnatal hippocampal neurogenesis and a reduction in the number of newborn neurons have been reported in other animal models of ASD.[67,68] Since NMDA receptor function is critical for the survival of newly born neurons,[69] the altered neurogenesis and reduced number of immature neurons observed in *Grin2b*$^{+/C456Y}$ mice could be a direct, cell-autonomous consequence of *Grin2b* LoF in granule neuroblasts. Alternatively, given that the activity of surrounding neurons could influence the survival of newly born neurons,[69] the reduction in DCX^{+} cells may result from altered neuronal activity in the hippocampus. In line with this possibility, we observed significant downregulation of activity-regulated genes in hippocampal excitatory neurons (Figure 5D). These findings point to dysregulated postnatal hippocampal neurogenesis as a potential mechanism contributing to ASD pathophysiology. Disrupted hippocampal neurogenesis has been linked to cognitive impairments and mood disorders and is associated with various psychiatric conditions, such as depression and ASD.[70] Interestingly, promoting the expansion of newborn neurons in the hippocampus has been shown to ameliorate ASD-like behaviors in mice,[71] highlighting the modulation of hippocampal neurogenesis as a potential therapeutic avenue for ASD.

It is noteworthy that the *Grin2b*$^{+/C456Y}$ brain transcriptomic phenotype is considerably different from that observed in *Grin2a*$^{+/-}$ mice. For instance, *Grin2b*$^{+/C456Y}$ mice showed early postnatal (2–4 weeks) dysregulation of energy metabolism and protein synthesis genes, aligning with the childhood onset of ASD.[72] In contrast, *Grin2a*$^{+/-}$ mice presented more prominent transcriptomic changes at 12 weeks,[42] which is more consistent with the peak onset of schizophrenia during adolescence and young adulthood.[73] These later-emerging transcriptomic effects were particularly evident in the TWI analysis of the PFC (Figure S8A), a region strongly implicated in schizophrenia pathophysiology.[74] The delayed developmental expression of *Grin2a*[75,76] may partly explain these spatiotemporal differences, particularly the absence of early postnatal energy metabolism alterations and the delayed emergence of changes in later-maturing regions such as the PFC[77] in *Grin2a*$^{+/-}$ mice. Together with the contrasting lack of striatal hyperdopaminergic state in *Grin2b* mutants, our study highlights the striking distinction between the neurobiological phenotypes of *Grin2a* and *Grin2b* heterozygous mutant mice. These brain phenotype differences, derived from unbiased -omics data, might help to explain why *GRIN2A* and *GRIN2B* have differential genetic associations with schizophrenia and ASD, despite encoding subunits of the same NMDAR.

Limitations of the study

An important limitation of this study is that changes in oxidative phosphorylation, protein synthesis, and neuronal activity are inferred from transcriptomic alterations. Functional assessments of energy metabolism and neuronal activity across developmental stages will therefore be crucial to fully understand the role of *Grin2b* in brain development.

Furthermore, while a few RNA processing and splicing factors (e.g., *Adarb2*) were detected among DEGs or abnormally spliced genes, the current dataset lacks sufficient power to identify changes at specific RNA editing sites or to accurately quantify alternative isoforms. Additional samples will be required to better characterize the scope and impact of splicing dysregulation and improve the gen-level analysis in *Grin2b* mutant mice.

The comparison between *Grin2a*$^{+/-}$ and *Grin2b*$^{+/C456Y}$ mutants provides valuable insight into shared and distinct transcriptomic effects of NMDAR subunit disruption. However, since haploinsufficiency and pathogenic missense mutations may have different molecular consequences, future studies using a *Grin2b* haploinsufficient model would allow a more direct mechanistic comparison with *Grin2a*$^{+/-}$ mice.

RESOURCE AVAILABILITY

Lead contact

Requests for further information and resources should be directed to and will be fulfilled by the lead contact, Zohreh Farsi (zfarsi@broadinstitute.org).

Materials availability

This study did not generate new unique reagents.

Data and code availability

- All bulk and single-nucleus RNA-seq data have been deposited at GEO (GSE312790) and are publicly available as of the date of publication. Supplemental tables and full DE tables for bulk RNA-seq analysis and pseudocell analysis of snRNA-seq data are available via Mendeley Data (https://doi.org/10.17632/g8454g4653.1). Accession numbers and DOIs are listed in the key resources table.
- All original code has been deposited on Terra Workspace (https://app.terra.bio/#workspaces/fbrihuman/sconline_integrative_analysis) and is publicly available as of the date of publication. DOIs are listed in the key resources table.
- Any additional information required to reanalyze the data reported in this article is available from the lead contact upon request.

ACKNOWLEDGMENTS

Research reported in this article was supported by the Stanley Center for Psychiatric Research and the Institute for Basic Science (IBS-R002-D1 to E.K.). We are grateful to Ajay Nadig for advice on TWI analysis, Broad Genomics Platform for sequencing, Vahid Gazestani for advice on pseudocell analysis, and Sameer Aryal and Bryan Song for discussions regarding the interpretation of the transcriptomics data.

AUTHOR CONTRIBUTIONS

Conceptualization, Z.F., M.S., and E.K.; formal analysis, A.N., S.K.S., Z.F., D.M., K.A.P., M.K., and G.L.; investigation, Z.F., N.S., W.S., M.K., G.L., M.J.K., K.S.B., I.P., and N.S.; resources, E.K. and M.S.; data curation, A.N., Z.F., D.M., K.A.P., M.K., and G.L.; writing – original draft, Z.F. and M.S. with inputs from all co-authors; writing – review and editing, Z.F.; visualization, Z.F., A.N., M.K., and G.L.; supervision, Z.F., M.S., E.K., and J.Z.L.; funding acquisition, M.S. and E.K.

DECLARATION OF INTERESTS

M.S. holds equity in Neumora Therapeutics, Illimis Therapeutics, Vanqua Bio, and is, or has been recently, a scientific advisor or consultant for Neumora, Illimis, and Curie.Bio, Astex Pharmaceuticals, Biogen.

STAR★METHODS

Detailed methods are provided in the online version of this paper and include the following:

SUPPLEMENTAL INFORMATION

Supplemental information can be found online at https://doi.org/10.1016/j.isci.2026.114700.

Received: September 8, 2025
Revised: November 12, 2025
Accepted: January 10, 2026
Published: January 15, 2026

REFERENCES

1. Zeidan, J., Fombonne, E., Scorah, J., Ibrahim, A., Durkin, M.S., Saxena, S., Yusuf, A., Shih, A., and Elsabbagh, M. (2022). Global prevalence of autism: A systematic review update. Autism Res. *15*, 778–790.
2. Feliciano, P., Zhou, X., Astrovskaya, I., Turner, T.N., Wang, T., Brueggeman, L., Barnard, R., Hsieh, A., Snyder, L.G., Muzny, D.M., et al. (2019). Exome sequencing of 457 autism families recruited online provides evidence for autism risk genes. NPJ Genom. Med. *4*, 19.
3. Glessner, J.T., Wang, K., Cai, G., Korvatska, O., Kim, C.E., Wood, S., Zhang, H., Estes, A., Brune, C.W., Bradfield, J.P., et al. (2009). Autism genome-wide copy number variation reveals ubiquitin and neuronal genes. Nature *459*, 569–573.
4. Ruzzo, E.K., Pérez-Cano, L., Jung, J.-Y., Wang, L.-K., Kashef-Haghighi, D., Hartl, C., Singh, C., Xu, J., Hoekstra, J.N., Leventhal, O., et al. (2019). Inherited and DE Novo genetic risk for autism impacts shared networks. Cell *178*, 850–866.e26.
5. Samocha, K.E., Robinson, E.B., Sanders, S.J., Stevens, C., Sabo, A., McGrath, L.M., Kosmicki, J.A., Rehnström, K., Mallick, S., Kirby, A., et al. (2014). A framework for the interpretation of de novo mutation in human disease. Nat. Genet. *46*, 944–950.
6. Satterstrom, F.K., Kosmicki, J.A., Wang, J., Breen, M.S., De Rubeis, S., An, J.-Y., Peng, M., Collins, R., Grove, J., Klei, L., et al. (2020). Large-Scale Exome Sequencing Study Implicates Both Developmental and Functional Changes in the Neurobiology of Autism. Cell *180*, 568–584.e23.
7. Wilfert, A.B., Turner, T.N., Murali, S.C., Hsieh, P., Sulovari, A., Wang, T., Coe, B.P., Guo, H., Hoekzema, K., Bakken, T.E., et al. (2021). Recent ultra-rare inherited variants implicate new autism candidate risk genes. Nat. Genet. *53*, 1125–1134.
8. C Yuen, R.K., Merico, D., Bookman, M., L Howe, J., Thiruvahindrapuram, B., Patel, R.V., Whitney, J., Deflaux, N., Bingham, J., Wang, Z., et al. (2017). Whole genome sequencing resource identifies 18 new candidate genes for autism spectrum disorder. Nat. Neurosci. *20*, 602–611.
9. Gaugler, T., Klei, L., Sanders, S.J., Bodea, C.A., Goldberg, A.P., Lee, A.B., Mahajan, M., Manaa, D., Pawitan, Y., Reichert, J., et al. (2014). Most genetic risk for autism resides with common variation. Nat. Genet. *46*, 881–885.
10. Iossifov, I., O'Roak, B.J., Sanders, S.J., Ronemus, M., Krumm, N., Levy, D., Stessman, H.A., Witherspoon, K.T., Vives, L., Patterson, K.E., et al. (2014). The contribution of de novo coding mutations to autism spectrum disorder. Nature *515*, 216–221.
11. Robinson, E.B., St Pourcain, B., Anttila, V., Kosmicki, J.A., Bulik-Sullivan, B., Grove, J., Maller, J., Samocha, K.E., Sanders, S.J., Ripke, S., et al.

(2016). Genetic risk for autism spectrum disorders and neuropsychiatric variation in the general population. Nat. Genet. *48*, 552–555.

12. Weiner, D.J., Wigdor, E.M., Ripke, S., Walters, R.K., Kosmicki, J.A., Grove, J., Samocha, K.E., Goldstein, J.I., Okbay, A., Bybjerg-Grauholm, J., et al. (2017). Polygenic transmission disequilibrium confirms that common and rare variation act additively to create risk for autism spectrum disorders. Nat. Genet. *49*, 978–985.
13. Fu, J.M., Satterstrom, F.K., Peng, M., Brand, H., Collins, R.L., Dong, S., Wamsley, B., Klei, L., Wang, L., Hao, S.P., et al. (2022). Rare coding variation provides insight into the genetic architecture and phenotypic context of autism. Nat. Genet. *54*, 1320–1331.
14. De Rubeis, S., He, X., Goldberg, A.P., Poultney, C.S., Samocha, K., Cicek, A.E., Kou, Y., Liu, L., Fromer, M., Walker, S., et al. (2014). Synaptic, transcriptional and chromatin genes disrupted in autism. Nature *515*, 209–215.
15. Myers, R.A., Casals, F., Gauthier, J., Hamdan, F.F., Keebler, J., Boyko, A.R., Bustamante, C.D., Piton, A.M., Spiegelman, D., Henrion, E., et al. (2011). A population genetic approach to mapping neurological disorder genes using deep resequencing. PLoS Genet. *7*, e1001318.
16. O'Roak, B.J., Vives, L., Fu, W., Egertson, J.D., Stanaway, I.B., Phelps, I.G., Carvill, G., Kumar, A., Lee, C., Ankenman, K., et al. (2012). Multiplex targeted sequencing identifies recurrently mutated genes in autism spectrum disorders. Science *338*, 1619–1622.
17. Iossifov, I., Levy, D., Allen, J., Ye, K., Ronemus, M., Lee, Y.-H., Yamrom, B., and Wigler, M. (2015). Low load for disruptive mutations in autism genes and their biased transmission. Proc. Natl. Acad. Sci. USA *112*, E5600–E5607.
18. Platzer, K., Yuan, H., Schütz, H., Winschel, A., Chen, W., Hu, C., Kusumoto, H., Heyne, H.O., Helbig, K.L., Tang, S., et al. (2017). GRIN2B encephalopathy: novel findings on phenotype, variant clustering, functional consequences and treatment aspects. J. Med. Genet. *54*, 460–470.
19. Lee, E.-J., Choi, S.Y., and Kim, E. (2015). NMDA receptor dysfunction in autism spectrum disorders. Curr. Opin. Pharmacol. *20*, 8–13.
20. Lee, S., Moon, H., and Kim, E. (2025). NMDAR dysfunction in autism spectrum disorders: Lessons learned from 10 years of study. Curr. Opin. Neurobiol. *92*, 103023.
21. Blundell, J., Blaiss, C.A., Etherton, M.R., Espinosa, F., Tabuchi, K., Walz, C., Bolliger, M.F., Südhof, T.C., and Powell, C.M. (2010). Neuroligin-1 deletion results in impaired spatial memory and increased repetitive behavior. J. Neurosci. *30*, 2115–2129.
22. Won, H., Lee, H.-R., Gee, H.Y., Mah, W., Kim, J.-I., Lee, J., Ha, S., Chung, C., Jung, E.S., Cho, Y.S., et al. (2012). Autistic-like social behaviour in Shank2-mutant mice improved by restoring NMDA receptor function. Nature *486*, 261–265.
23. Chung, W., Choi, S.Y., Lee, E., Park, H., Kang, J., Park, H., Choi, Y., Lee, D., Park, S.-G., Kim, R., et al. (2015). Social deficits in IRSp53 mutant mice improved by NMDAR and mGluR5 suppression. Nat. Neurosci. *18*, 435–443.
24. Chung, C., Ha, S., Kang, H., Lee, J., Um, S.M., Yan, H., Yoo, Y.-E., Yoo, T., Jung, H., Lee, D., et al. (2019). Early correction of N-methyl-D-aspartate receptor function improves autistic-like social behaviors in adult Shank2−/− mice. Biol. Psychiatry *85*, 534–543.
25. Duffney, L.J., Zhong, P., Wei, J., Matas, E., Cheng, J., Qin, L., Ma, K., Dietz, D.M., Kajiwara, Y., Buxbaum, J.D., and Yan, Z. (2015). Autism-like deficits in Shank3-deficient mice are rescued by targeting actin regulators. Cell Rep. *11*, 1400–1413.
26. Kutsuwada, T., Sakimura, K., Manabe, T., Takayama, C., Katakura, N., Kushiya, E., Natsume, R., Watanabe, M., Inoue, Y., Yagi, T., et al. (1996). Impairment of suckling response, trigeminal neuronal pattern formation, and hippocampal LTD in NMDA receptor epsilon 2 subunit mutant mice. Neuron *16*, 333–344.
27. Sprengel, R., Suchanek, B., Amico, C., Brusa, R., Burnashev, N., Rozov, A., Hvalby, O., Jensen, V., Paulsen, O., Andersen, P., et al. (1998). Importance of the intracellular domain of NR2 subunits for NMDA receptor function in vivo. Cell *92*, 279–289.
28. Brigman, J.L., Wright, T., Talani, G., Prasad-Mulcare, S., Jinde, S., Seabold, G.K., Mathur, P., Davis, M.I., Bock, R., Gustin, R.M., et al. (2010). Loss of GluN2B-containing NMDA receptors in CA1 hippocampus and cortex impairs long-term depression, reduces dendritic spine density, and disrupts learning. J. Neurosci. *30*, 4590–4600.
29. von Engelhardt, J., Doganci, B., Jensen, V., Hvalby, Ø., Göngrich, C., Taylor, A., Barkus, C., Sanderson, D.J., Rawlins, J.N.P., Seeburg, P.H., et al. (2008). Contribution of hippocampal and extra-hippocampal NR2B-containing NMDA receptors to performance on spatial learning tasks. Neuron *60*, 846–860.
30. Akashi, K., Kakizaki, T., Kamiya, H., Fukaya, M., Yamasaki, M., Abe, M., Natsume, R., Watanabe, M., and Sakimura, K. (2009). NMDA receptor GluN2B (GluR epsilon 2/NR2B) subunit is crucial for channel function, postsynaptic macromolecular organization, and actin cytoskeleton at hippocampal CA3 synapses. J. Neurosci. *29*, 10869–10882.
31. Shin, W., Kim, K., Serraz, B., Cho, Y.S., Kim, D., Kang, M., Lee, E.-J., Lee, H., Bae, Y.C., Paoletti, P., and Kim, E. (2020). Early correction of synaptic long-term depression improves abnormal anxiety-like behavior in adult GluN2B-C456Y-mutant mice. PLoS Biol. *18*, e3000717.
32. Lee, S., Jung, W.B., Moon, H., Im, G.H., Noh, Y.W., Shin, W., Kim, Y.G., Yi, J.H., Hong, S.J., Jung, Y., et al. (2024). Anterior cingulate cortex-related functional hyperconnectivity underlies sensory hypersensitivity in Grin2b-mutant mice. Mol. Psychiatry *29*, 3195–3207.
33. Chang, J., Gilman, S.R., Chiang, A.H., Sanders, S.J., and Vitkup, D. (2015). Genotype to phenotype relationships in autism spectrum disorders. Nat. Neurosci. *18*, 191–198.
34. Ramaswami, G., Won, H., Gandal, M.J., Haney, J., Wang, J.C., Wong, C.C.Y., Sun, W., Prabhakar, S., Mill, J., and Geschwind, D.H. (2020). Integrative genomics identifies a convergent molecular subtype that links epigenomic with transcriptomic differences in autism. Nat. Commun. *11*, 4873.
35. Velmeshev, D., Schirmer, L., Jung, D., Haeussler, M., Perez, Y., Mayer, S., Bhaduri, A., Goyal, N., Rowitch, D.H., and Kriegstein, A.R. (2019). Single-cell genomics identifies cell type-specific molecular changes in autism. Science *364*, 685–689.
36. Voineagu, I., Wang, X., Johnston, P., Lowe, J.K., Tian, Y., Horvath, S., Mill, J., Cantor, R.M., Blencowe, B.J., and Geschwind, D.H. (2011). Transcriptomic analysis of autistic brain reveals convergent molecular pathology. Nature *474*, 380–384.
37. Garbett, K., Ebert, P.J., Mitchell, A., Lintas, C., Manzi, B., Mirnics, K., and Persico, A.M. (2008). Immune transcriptome alterations in the temporal cortex of subjects with autism. Neurobiol. Dis. *30*, 303–311.
38. Parikshak, N.N., Luo, R., Zhang, A., Won, H., Lowe, J.K., Chandran, V., Horvath, S., and Geschwind, D.H. (2013). Integrative functional genomic analyses implicate specific molecular pathways and circuits in autism. Cell *155*, 1008–1021.
39. Parikshak, N.N., Swarup, V., Belgard, T.G., Irimia, M., Ramaswami, G., Gandal, M.J., Hartl, C., Leppa, V., Ubieta, L.d.l.T., Huang, J., et al. (2016). Genome-wide changes in lncRNA, splicing, and regional gene expression patterns in autism. Nature *540*, 423–427.
40. Gupta, S., Ellis, S.E., Ashar, F.N., Moes, A., Bader, J.S., Zhan, J., West, A.B., and Arking, D.E. (2014). Transcriptome analysis reveals dysregulation of innate immune response genes and neuronal activity-dependent genes in autism. Nat. Commun. *5*, 5748.
41. Krishnan, A., Zhang, R., Yao, V., Theesfeld, C.L., Wong, A.K., Tadych, A., Volfovsky, N., Packer, A., Lash, A., and Troyanskaya, O.G. (2016). Genome-wide prediction and functional characterization of the genetic basis of autism spectrum disorder. Nat. Neurosci. *19*, 1454–1462.

42. Farsi, Z., Nicolella, A., Simmons, S.K., Aryal, S., Shepard, N., Brenner, K., Lin, S., Herzog, L., Moran, S.P., Stalnaker, K.J., et al. (2023). Brain-region-specific changes in neurons and glia and dysregulation of dopamine signaling in Grin2a mutant mice. Neuron *111*, 3378–3396.e9.

43. Nadig, A., Replogle, J.M., Pogson, A.N., Murthy, M., McCarroll, S.A., Weissman, J.S., Robinson, E.B., and O'Connor, L.J. (2025). Transcriptome-wide analysis of differential expression in perturbation atlases. Nat. Genet. *57*, 1228–1237.

44. Zhang, P., Omanska, A., Ander, B.P., Gandal, M.J., Stamova, B., and Schumann, C.M. (2023). Neuron-specific transcriptomic signatures indicate neuroinflammation and altered neuronal activity in ASD temporal cortex. Proc. Natl. Acad. Sci. USA *120*, e2206758120.

45. Gandal, M.J., Haney, J.R., Wamsley, B., Yap, C.X., Parhami, S., Emani, P.S., Chang, N., Chen, G.T., Hoftman, G.D., de Alba, D., et al. (2022). Broad transcriptomic dysregulation occurs across the cerebral cortex in ASD. Nature *611*, 532–539.

46. Underwood, J.G., Boutz, P.L., Dougherty, J.D., Stoilov, P., and Black, D.L. (2005). Homologues of the Caenorhabditis elegans Fox-1 protein are neuronal splicing regulators in mammals. Mol. Cell Biol. *25*, 10005–10016.

47. Martin, C.L., Duvall, J.A., Ilkin, Y., Simon, J.S., Arreaza, M.G., Wilkes, K., Alvarez-Retuerto, A., Whichello, A., Powell, C.M., Rao, K., et al. (2007). Cytogenetic and molecular characterization of A2BP1/FOX1 as a candidate gene for autism. Am. J. Med. Genet. B Neuropsychiatr. Genet. *144B*, 869–876.

48. Bill, B.R., Lowe, J.K., Dybuncio, C.T., and Fogel, B.L. (2013). Orchestration of neurodevelopmental programs by RBFOX1: implications for autism spectrum disorder. Int. Rev. Neurobiol. *113*, 251–267.

49. Weyn-Vanhentenryck, S.M., Mele, A., Yan, Q., Sun, S., Farny, N., Zhang, Z., Xue, C., Herre, M., Silver, P.A., Zhang, M.Q., et al. (2014). HITS-CLIP and integrative modeling define the Rbfox splicing-regulatory network linked to brain development and autism. Cell Rep. *6*, 1139–1152.

50. Zhang, C., Zhang, Z., Castle, J., Sun, S., Johnson, J., Krainer, A.R., and Zhang, M.Q. (2008). Defining the regulatory network of the tissue-specific splicing factors Fox-1 and Fox-2. Genes Dev. *22*, 2550–2563.

51. Singh, T., Poterba, T., Curtis, D., Akil, H., Al Eissa, M., Barchas, J.D., Bass, N., Bigdeli, T.B., Breen, G., Bromet, E.J., et al. (2022). Rare coding variants in ten genes confer substantial risk for schizophrenia. Nature *604*, 509–516.

52. Aryal, S., Geng, C., Kwon, M.J., Farsi, Z., Goble, N., Asan, A.S., Brenner, K., Shepard, N., Seidel, O., Wang, Y., et al. (2024). Reduction of SynGAP-γ, disrupted splicing of *Agap3*, and oligodendrocyte deficits in *Srrm2* mice, a genetic model of schizophrenia and neurodevelopmental disorder. Preprint at bioRxiv. https://doi.org/10.1101/2024.10.10.617460.

53. Gazestani, V., Kamath, T., Nadaf, N.M., Dougalis, A., Burris, S.J., Rooney, B., Junkkari, A., Vanderburg, C., Pelkonen, A., Gomez-Budia, M., et al. (2023). Early Alzheimer's disease pathology in human cortex involves transient cell states. Cell *186*, 4438–4453.e23.

54. Tyssowski, K.M., DeStefino, N.R., Cho, J.-H., Dunn, C.J., Poston, R.G., Carty, C.E., Jones, R.D., Chang, S.M., Romeo, P., Wurzelmann, M.K., et al. (2018). Different Neuronal Activity Patterns Induce Different Gene Expression Programs. Neuron *98*, 530–546.e11.

55. Lau, W.K.W., Leung, M.-K., and Lau, B.W.M. (2019). Resting-state abnormalities in Autism Spectrum Disorders: A meta-analysis. Sci. Rep. *9*, 3892.

56. Kosillo, P., and Bateup, H.S. (2021). Dopaminergic dysregulation in syndromic autism spectrum disorders: Insights from genetic mouse models. Front. Neural Circuits *15*, 700968.

57. Khaliulin, I., Hamoudi, W., and Amal, H. (2025). The multifaceted role of mitochondria in autism spectrum disorder. Mol. Psychiatry *30*, 629–650.

58. Li, Q., Lee, J.-A., and Black, D.L. (2007). Neuronal regulation of alternative pre-mRNA splicing. Nat. Rev. Neurosci. *8*, 819–831.

59. Iijima, T., Wu, K., Witte, H., Hanno-Iijima, Y., Glatter, T., Richard, S., and Scheiffele, P. (2011). SAM68 regulates neuronal activity-dependent alternative splicing of neurexin-1. Cell *147*, 1601–1614.

60. Irimia, M., Weatheritt, R.J., Ellis, J.D., Parikshak, N.N., Gonatopoulos-Pournatzis, T., Babor, M., Quesnel-Vallières, M., Tapial, J., Raj, B., O'Hanlon, D., et al. (2014). A highly conserved program of neuronal microexons is misregulated in autistic brains. Cell *159*, 1511–1523.

61. Velmeshev, D., Magistri, M., Mazza, E.M.C., Lally, P., Khoury, N., D'Elia, E.R., Bicciato, S., and Faghihi, M.A. (2020). Cell-type-specific analysis of molecular pathology in autism identifies common genes and pathways affected across neocortical regions. Mol. Neurobiol. *57*, 2279–2289.

62. Gandal, M.J., Zhang, P., Hadjimichael, E., Walker, R.L., Chen, C., Liu, S., Won, H., van Bakel, H., Varghese, M., Wang, Y., et al. (2018). Transcriptome-wide isoform-level dysregulation in ASD, schizophrenia, and bipolar disorder. Science *362*, eaat8127. https://doi.org/10.1126/science.aat8127.

63. Engal, E., Zhang, Z., Geminder, O., Jaffe-Herman, S., Kay, G., Ben-Hur, A., and Salton, M. (2024). The spectrum of pre-mRNA splicing in autism. Wiley Interdiscip. Rev. RNA *15*, e1838.

64. Chau, K.K., Zhang, P., Urresti, J., Amar, M., Pramod, A.B., Chen, J., Thomas, A., Corominas, R., Lin, G.N., and Iakoucheva, L.M. (2021). Full-length isoform transcriptome of the developing human brain provides further insights into autism. Cell Rep. *36*, 109631.

65. Xu, X., Wang, J., Hu, K., Su, D., Huang, Q., Fan, X., and Fan, X. (2024). Single-cell full-length isoform sequencing unveils transcriptional dysregulation in autism spectrum disorder during cerebral cortex development. Preprint at bioRxiv. https://doi.org/10.1101/2024.12.04.626807.

66. van de Leemput, J., Boles, N.C., Kiehl, T.R., Corneo, B., Lederman, P., Menon, V., Lee, C., Martinez, R.A., Levi, B.P., Thompson, C.L., et al. (2014). CORTECON: a temporal transcriptome analysis of in vitro human cerebral cortex development from human embryonic stem cells. Neuron *83*, 51–68.

67. Barón-Mendoza, I., Mejía-Hernández, M., Hernández-Mercado, K., Guzmán-Condado, J., Zepeda, A., and González-Arenas, A. (2024). Altered hippocampal neurogenesis in a mouse model of autism revealed by genetic polymorphisms and by atypical development of newborn neurons. Sci. Rep. *14*, 4608.

68. Stephenson, D.T., O'Neill, S.M., Narayan, S., Tiwari, A., Arnold, E., Samaroo, H.D., Du, F., Ring, R.H., Campbell, B., Pletcher, M., et al. (2011). Histopathologic characterization of the BTBR mouse model of autistic-like behavior reveals selective changes in neurodevelopmental proteins and adult hippocampal neurogenesis. Mol. Autism *2*, 7.

69. Tashiro, A., Sandler, V.M., Toni, N., Zhao, C., and Gage, F.H. (2006). NMDA-receptor-mediated, cell-specific integration of new neurons in adult dentate gyrus. Nature *442*, 929–933.

70. Liu, C., Liu, J., Gong, H., Liu, T., Li, X., and Fan, X. (2023). Implication of hippocampal neurogenesis in autism spectrum disorder: Pathogenesis and therapeutic implications. Curr. Neuropharmacol. *21*, 2266–2282.

71. Meng, H., Li, Q., Wang, J., Yue, W., Zhang, D., Sun, X., Wang, L., and Li, J. (2023). The expansion of newborn neurons in hippocampus improves social recognition deficit in a mouse model of autism. Front. Psychiatry *14*, 1162179.

72. Solmi, M., Song, M., Yon, D.K., Lee, S.W., Fombonne, E., Kim, M.S., Park, S., Lee, M.H., Hwang, J., Keller, R., et al. (2022). Incidence, prevalence, and global burden of autism spectrum disorder from 1990 to 2019 across 204 countries. Mol. Psychiatry *27*, 4172–4180.

73. Uhlhaas, P.J., Davey, C.G., Mehta, U.M., Shah, J., Torous, J., Allen, N.B., Avenevoli, S., Bella-Awusah, T., Chanen, A., Chen, E.Y.H., et al. (2023). Towards a youth mental health paradigm: a perspective and roadmap. Mol. Psychiatry *28*, 3171–3181.

74. Sakurai, T., Gamo, N.J., Hikida, T., Kim, S.-H., Murai, T., Tomoda, T., and Sawa, A. (2015). Converging models of schizophrenia–Network

alterations of prefrontal cortex underlying cognitive impairments. Prog. Neurobiol. *134*, 178–201.

75. Paoletti, P., Bellone, C., and Zhou, Q. (2013). NMDA receptor subunit diversity: impact on receptor properties, synaptic plasticity and disease. Nat. Rev. Neurosci. *14*, 383–400.
76. Sheng, M., Cummings, J., Roldan, L.A., Jan, Y.N., and Jan, L.Y. (1994). Changing subunit composition of heteromeric NMDA receptors during development of rat cortex. Nature *368*, 144–147.
77. Kolk, S.M., and Rakic, P. (2022). Development of prefrontal cortex. Neuropsychopharmacology *47*, 41–57.
78. Li, B., and Dewey, C.N. (2011). RSEM: accurate transcript quantification from RNA-Seq data with or without a reference genome. BMC Bioinf. *12*, 323.
79. Love, M.I., Huber, W., and Anders, S. (2014). Moderated estimation of fold change and dispersion for RNA-Seq data with DESeq2. Preprint at bioRxiv. https://doi.org/10.1101/002832.
80. Stuart, T., Butler, A., Hoffman, P., Hafemeister, C., Papalexi, E., Mauck, W.M., Hao, Y., Stoeckius, M., Smibert, P., and Satija, R. (2019). Comprehensive integration of single-cell data. Cell *177*, 1888–1902.e21.
81. Wolock, S.L., Lopez, R., and Klein, A.M. (2019). Scrublet: Computational identification of cell Doublets in Single-cell transcriptomic data. Cell Syst. *8*, 281–291.e9.
82. Hao, Y., Hao, S., Andersen-Nissen, E., Mauck, W.M., 3rd, Zheng, S., Butler, A., Lee, M.J., Wilk, A.J., Darby, C., Zager, M., et al. (2021). Integrated analysis of multimodal single-cell data. Cell *184*, 3573–3587.e29.
83. Phipson, B., Sim, C.B., Porrello, E.R., Hewitt, A.W., Powell, J., and Oshlack, A. (2022). Propeller: Testing for differences in cell type proportions in single cell data. Bioinformatics *38*, 4720–4726.
84. Robinson, M.D., McCarthy, D.J., and Smyth, G.K. (2010). edgeR: a Bioconductor package for differential expression analysis of digital gene expression data. Bioinformatics *26*, 139–140.
85. Korotkevich, G., Sukhov, V., Budin, N., Shpak, B., Artyomov, M.N., and Sergushichev, A. (2016). Fast gene set enrichment analysis. Preprint at bioRxiv. https://doi.org/10.1101/060012.
86. Harris, C.R., Millman, K.J., van der Walt, S.J., Gommers, R., Virtanen, P., Cournapeau, D., Wieser, E., Taylor, J., Berg, S., Smith, N.J., et al. (2020). Array programming with NumPy. Nature *585*, 357–362.
87. McKinney, W. (2010). Data Structures for Statistical Computing in Python. In Proceedings of the Python in Science Conference (SciPy), pp. 56–61.
88. Virtanen, P., Gommers, R., Oliphant, T.E., Haberland, M., Reddy, T., Cournapeau, D., Burovski, E., Peterson, P., Weckesser, W., Bright, J., et al. (2020). SciPy 1.0: fundamental algorithms for scientific computing in Python. Nat. Methods *17*, 261–272.
89. Hunter, J.D. (2007). Matplotlib: A 2D Graphics Environment. Comput. Sci. Eng. *9*, 90–95.
90. Patro, R., Duggal, G., Love, M.I., Irizarry, R.A., and Kingsford, C. (2017). Salmon provides fast and bias-aware quantification of transcript expression. Nat. Methods *14*, 417–419.
91. Dobin, A., Davis, C.A., Schlesinger, F., Drenkow, J., Zaleski, C., Jha, S., Batut, P., Chaisson, M., and Gingeras, T.R. (2013). STAR: ultrafast universal RNA-seq aligner. Bioinformatics *29*, 15–21.
92. Liao, Y., Smyth, G.K., and Shi, W. (2014). featureCounts: an efficient general purpose program for assigning sequence reads to genomic features. Bioinformatics *30*, 923–930.
93. Ahlmann-Eltze, C., and Huber, W. (2021). glmGamPoi: fitting Gamma-Poisson generalized linear models on single cell count data. Bioinformatics *36*, 5701–5702.
94. Yao, Z., van Velthoven, C.T.J., Nguyen, T.N., Goldy, J., Sedeno-Cortes, A.E., Baftizadeh, F., Bertagnolli, D., Casper, T., Chiang, M., Crichton, K., et al. (2021). A taxonomy of transcriptomic cell types across the isocortex and hippocampal formation. Cell *184*, 3222–3241.e26.
95. Saunders, A., Macosko, E.Z., Wysoker, A., Goldman, M., Krienen, F.M., de Rivera, H., Bien, E., Baum, M., Bortolin, L., Wang, S., et al. (2018). Molecular Diversity and Specializations among the Cells of the Adult Mouse Brain. Cell *174*, 1015–1030.e16.
96. Yao, Z., Liu, H., Xie, F., Fischer, S., Adkins, R.S., Aldridge, A.I., Ament, S.A., Bartlett, A., Behrens, M.M., Van den Berge, K., et al. (2021). A transcriptomic and epigenomic cell atlas of the mouse primary motor cortex. Nature *598*, 103–110.
97. Biancalani, T., Scalia, G., Buffoni, L., Avasthi, R., Lu, Z., Sanger, A., Tokcan, N., Vanderburg, C.R., Segerstolpe, Å., Zhang, M., et al. (2021). Deep learning and alignment of spatially resolved single-cell transcriptomes with Tangram. Nat. Methods *18*, 1352–1362.
98. Langfelder, P., and Horvath, S. (2008). WGCNA: an R package for weighted correlation network analysis. BMC Bioinf. *9*, 559.
99. Mandell, K.A.P., Simmons, S.K., Nadig, A., Farsi, Z., Huang, W.-C., Aryal, S., Kwon, M.J., Song, B., Brenner, K., Shepard, N., et al. (2025). Meta-analysis of the brain transcriptomes of multiple genetic mouse models of schizophrenia highlights dysregulation in striatum and thalamus. Preprint at bioRxiv. https://doi.org/10.1101/2025.03.26.645496.
100. Leek, J.T., and Storey, J.D. (2007). Capturing heterogeneity in gene expression studies by surrogate variable analysis. PLoS Genet. *3*, 1724–1735.
101. Zheng, G.X.Y., Terry, J.M., Belgrader, P., Ryvkin, P., Bent, Z.W., Wilson, R., Ziraldo, S.B., Wheeler, T.D., McDermott, G.P., Zhu, J., et al. (2017). Massively parallel digital transcriptional profiling of single cells. Nat. Commun. *8*, 14049.
102. Ding, J., Adiconis, X., Simmons, S.K., Kowalczyk, M.S., Hession, C.C., Marjanovic, N.D., Hughes, T.K., Wadsworth, M.H., Burks, T., Nguyen, L.T., et al. (2020). Author Correction: Systematic comparison of single-cell and single-nucleus RNA-sequencing methods. Nat. Biotechnol. *38*, 756.
103. Zeisel, A., Hochgerner, H., Lönnerberg, P., Johnsson, A., Memic, F., van der Zwan, J., Häring, M., Braun, E., Borm, L.E., La Manno, G., et al. (2018). Molecular Architecture of the Mouse Nervous System. Cell *174*, 999–1014.e22.
104. Law, C.W., Chen, Y., Shi, W., and Smyth, G.K. (2014). voom: Precision weights unlock linear model analysis tools for RNA-seq read counts. Genome Biol. *15*, R29.
105. Subramanian, A., Tamayo, P., Mootha, V.K., Mukherjee, S., Ebert, B.L., Gillette, M.A., Paulovich, A., Pomeroy, S.L., Golub, T.R., Lander, E.S., and Mesirov, J.P. (2005). Gene set enrichment analysis: a knowledge-based approach for interpreting genome-wide expression profiles. Proc. Natl. Acad. Sci. USA *102*, 15545–15550.

STAR★METHODS

KEY RESOURCES TABLE

REAGENT or RESOURCE	SOURCE	IDENTIFIER
Antibodies		
Rabbit anti-Doublecortin	Abcam	Cat# ab18723; RRID: AB_732011
Rat anti-Ki-67, FITC-conjugated	Thermofisher	Cat# 11-5698-82; RRID: AB_11151330
anti-rabbit Alexa Fluor 594	Jackson	Cat# 711-586-152; RRID: AB_2340622
Experimental models: Organisms/strains		
Mouse: *Grin2b*$^{+/C456Y}$ mutant mice	Shin et al.[31]	RRID: IMSR_JAX:039026
Critical commercial assays		
RNeasy Mini Kit	Qiagen	Cat# 74106
TruSeq Stranded mRNA Kit	Illumina	Cat# 20020595
NextGEM SC 3′ LibGel v3.1 Kit	10x Genomics	Cat# 1000268
Dual Index Kit TT Set A	10x Genomics	Cat# 1000215
Deposited data		
Raw and processed bulk RNA-seq data of Substantia Nigra from *Grin2a* and *Grin2b* mutant mice; Raw and processed single-nucleus RNA-seq data from *Grin2b* mutant mice	This paper	GEO: GSE312790
Raw and processed bulk RNA-seq data for PFC, Hippocampus, Somatosensory Cortex, Striatum and Thalamus of *Grin2b* and *Grin2a* mutant mice	Farsi et al.[42]	GEO: GSE218573
Analyzed DE and GSEA data of all brain regions and ages (bulk and single-nucleus RNA-seq) from *Grin2b* mutant mice as well as DE data of Substantia Nigra from *Grin2a* mutant mice	This paper	Tables S2–S5, S7, and S8; Mendeley Data: https://doi.org/10.17632/g8454g4653.1
Analyzed DE and GSEA data of all brain regions (except for Substantia Nigra) and ages (bulk and single-nucleus RNA-seq) from *Grin2a* mutant mice	Farsi et al.[42]	Mendeley Data: https://doi.org/10.17632/d5t8dtnmx4.1
Software and algorithms		
CellRanger v3.0.2	10x Genomics	RRID: SCR_017344
RSEM v1.3.0	Li et al.[78]	RRID: SCR_013027
DESeq2 v1.20.0	Love et al.[79]	RRID: SCR_015687
Seurat v3.2.3	Stuart et al.[80]	RRID: SCR_016341
Scrublet v0.2.3	Wolock et al.[81]	RRID: SCR_018098
Azimuth	Hao et al.[82]	RRID: SCR_021084
Speckle v0.0.3	Phipson et al.[83]	https://github.com/phipsonlab/speckle
EdgeR v3.22.3	Robinson et al.[84]	RRID: SCR_012802
fGSEA v1.16.0	Korotkevich et al.[85]	RRID: SCR_020938
MATLAB	Mathworks	RRID: SCR_001622
R v4.1.3	The R Foundation	RRID: SCR_001905
Python v3.11.6	Python Software Foundation	RRID: SCR_008394
Numpy	Harris et al.[86]	RRID: SCR_008633
Pandas	McKinney et al.[87]	RRID: SCR_018214
Scipy	Virtanen et al.[88]	RRID: SCR_008058
Matplotlib	Hunter et al.[89]	RRID: SCR_008624
Salmon	Patro et al.[90]	RRID: SCR_017036

(*Continued on next page*)

Continued

REAGENT or RESOURCE	SOURCE	IDENTIFIER
STARd	Dobin et al.[91]	RRID: SCR_004463
featureCoun	Liao et al.[92]	RRID: SCR_012919
PICARDTools	https://broadinstitute.github.io/picard/	RRID: SCR_006525
glmGamPoi	Ahlmann-Eltze and Huber.[93]	https://github.com/const-ae/glmGamPoi
GraphPad Prism	GraphPad	RRID: SCR_002798
ImageJ	NIH, Wayne Rasband	RRID: SCR_003070
All original code	This paper	Pseudocell: https://app.terra.bio/#workspaces/fbrihuman/sconline_integrative_analysis
Other		
Allen Brain Atlas "WHOLE CORTEX & HIPPOCAMPUS – 10X GENOMICS"	Yao et al.[94]	https://portal.brain-map.org/atlases-and-data/rnaseq/mouse-whole-cortex-and-hippocampus-10x
DropViz "annotation.BrainCellAtlas_Saunders_version_2018.04.01.rds"	Saunders at al.[95]	http://dropviz.org/
Azimuth Mouse Motor Cortex	Yao et al.[96]	https://zenodo.org/record/4546935

EXPERIMENTAL MODEL AND STUDY PARTICIPANT DETAILS

Grin2b$^{+/C456Y}$ mice[31] were maintained on the C57BL/6J background. All mice were bred and housed in individually ventilated cages under controlled temperature and humidity. All procedures were approved by the KAIST Institutional Animal Care and Use Committee (KA2020-90). Frozen whole brain tissues of *Grin2b*$^{+/C456Y}$ mutant mice and wild-type littermates were generously shipped to the Broad Institute of MIT and Harvard for transcriptomics analyses.

METHOD DETAILS

Brain perfusions and tissue dissections

To generate samples for bulk and single-nucleus RNA sequencing (snRNA-seq), we followed an established protocol published on protocols.io (https://www.protocols.io/view/fresh-frozen-mouse-brain-preparation-for-single-nu-bcbrism6). To control for sex-based variability, only male mice were included in the experimental cohort. Male *Grin2b*$^{+/-}$ and wild-type littermates were anesthetized at 2, 4, 12, and 20 weeks of age using isoflurane administered in an induction chamber. Anesthesia was maintained using a nose cone delivering 3% isoflurane during the procedure. Animals underwent transcardial perfusion with ice-cold Hank's Balanced Salt Solution (HBSS) to flush blood from the vasculature. Brains were flash-frozen by placing them in liquid nitrogen vapor for 3 min and subsequently stored at −80°C.

Tissue sectioning was conducted within a Leica CM3050S cryostat. All dissection instruments were prechilled to −20 °C prior to use. The cerebellum was cut in the coronal plane with a razor blade cooled to −20 °C. Each brain was cut along the midsagittal axis to allow the right and left hemisphere to be allocated for bulk RNA-seq and snRNA-seq analysis, respectively. For prefrontal cortex (PFC) isolation, each hemisphere was mounted lateral side down onto a cryostat chuck using O.C.T. (optimal cutting temperature) compound (Tissue-Tek), ensuring the medial surface remained undisturbed by the embedding process. The PFC was dissected manually under cold conditions using a pre-cooled ophthalmic microscalpel (Feather Safety Razor, no. P-715). To isolate the remaining brain structures, the remaining tissue was removed from the O.C.T and repositioned with the olfactory bulb mounted face down on a fresh chuck using O.C.T. Serial coronal trimming was carried out in 30 μm increments until the ventral hippocampus became visible, then substantia nigra was obtained with a 0.15 cm diameter biopsy punch (Thermo Fisher Scientific), also prechilled to −20 °C. Sectioning continued until the dorsal hippocampus became visible, a gradual approach intended to minimize mechanical disruption of surface architecture. The hippocampus was dissected manually, while the thalamus was obtained with a 0.15 cm diameter biopsy punch. Again sectioning continued until the lateral ventricles acquired a triangular appearance, at which point the somatosensory cortex was dissected with the ophthalmic microscalpel and the dorsal striatum was sampled using another biopsy punch. All anatomical references were guided by the Allen Brain Atlas. Isolated tissues were placed in pre-cooled 1.5 mL PCR tubes and stored at −80 °C.

RNA isolation and bulk RNA-seq library preparation

Total RNA was extracted from the microdissected regions using the RNeasy Mini Kit (Qiagen), following the manufacturer's protocol. Samples were lysed and homogenized, and RNA was purified through silica-membrane spin columns. Residual DNA was removed by on-column DNase treatment (Qiagen), followed by elution in RNase-free water. Concentration measurements were performed

with a NanoDrop spectrophotometer, and RNA quality was assessed using Agilent RNA Pico Chips on a 2100 Bioanalyzer system. Extracted RNA was stored at −80 °C until further processing.

For bulk sequencing, libraries were prepared using the TruSeq Stranded mRNA Kit (Illumina) per the manufacturer's instructions. For each sample, 200 ng of total RNA was used as input. Final cDNA libraries were quantified using High Sensitivity DNA Chips (Agilent) on the Agilent 2100 Bioanalyzer. Libraries were pooled at a normalized concentration of 10 nM and sequenced on the Illumina NovaSeq 6000 S2 platform, employing paired-end reads of 50 bases each, with dual 8-base index reads. Average number of reads per brain region and genotype can be found in Table S1.

Nuclei isolation and single-nucleus RNA-seq library preparation

To prevent degradation from freeze-thaw stress, nuclei isolation was performed immediately after cryosectioning. A gentle detergent-based lysis protocol was used for nuclear extraction, as described previously[97] and accessible online (https://www.protocols.io/view/frozen-tissue-nuclei-extraction-bbseinbe). Isolated nuclei were loaded into the Chromium Controller (10,000 nuclei per channel) using the v3.1 chemistry (10x Genomics), and library generation proceeded according to the manufacturer's workflow. Libraries were pooled after normalization to 10 nM and sequenced on an Illumina NovaSeq 6000 S2 platform. Read configuration included 28 bases for Read 1, 75 bases for Read 2, and 10 bases for each of the dual index reads. At least 20,000 read pairs per nucleus were obtained.

Immunohistochemistry

Immunohistochemistry was performed to evaluate neurogenesis in the dentate gyrus (DG) and oligodendrocyte progenitor cell (OPC) density in the hippocampus of 4-week *Grin2b* mutant mice. Mice were anesthetized with isoflurane (Terrell) and transcardially perfused with 50 mL of heparinized phosphate-buffered saline (PBS), followed by 50 mL of 4% paraformaldehyde (PFA). Brains were extracted and post-fixed in 4% PFA overnight at 4 °C, then washed three times in PBS. Coronal sections (50 μm thickness) were prepared using a vibratome (VT1200s, Leica) and stored in PBS. To reduce nonspecific antibody binding and permeabilize the tissue, sections were incubated at 4 °C for 1 h in a blocking solution containing 5% normal donkey serum (S30, Millipore) and 0.2% Triton X-100 (0694, Amresco) in PBS. They were then incubated overnight at 4 °C with the following primary antibodies: DCX (ab18723; Abcam; 1:1000), Ki-67 (FITC-conjugated; 11-5698-82, Thermofisher; 1:250). After primary antibody incubation, sections were washed five times in blocking solution, then incubated for 3 h at room temperature with anti-rabbit Alexa Fluor 594 (1:500) for DCX. All steps involving antibodies were conducted in darkness to prevent photobleaching. Following incubation with the secondary antibody, sections were washed five times in blocking solution and mounted using a DAPI-containing mounting medium (H-1200-10, Vector Laboratories). Imaging was performed on an Axio Scan.Z1 slide scanner, and ImageJ software was used to automatically quantify the number of DCX- and Ki-67-positive cells.

QUANTIFICATION AND STATISTICAL ANALYSIS

Bulk RNA-seq data analysis

We performed a re-analysis of previously published bulk RNA-seq data (deposited at GEO: GSE218573) for five brain regions of *Grin2a* and *Grin2b* mutant mice, including the prefrontal cortex (PFC), hippocampus (HP), somatosensory cortex (SSC), striatum (ST), and thalamus (TH).[42] For the substantia nigra (SN) from *Grin2a* and *Grin2b* mutant mice, differential expression analysis was conducted across four postnatal ages, as described later in discussion.

Starting with FASTQ files, we used RSEM v1.3.0[78] to estimate gene and isoform level expression values for each bulk RNA-seq sample. The rsem-prepare-reference program was used with default parameters to generate the M25 (GRCm38.p6) GENCODE reference used for alignment. rsem-calculate-expression was used to calculate expression values with the following flags: –bowtie2, –paired-end, –estimate-rspd, –append-names, and –sort-bam-by-coordinate. Principal component analysis (PCA) was performed for each age and brain region pairing as a quality control measure to identify outlier samples for removal. The number of samples analyzed across different brain regions, age groups and genotypes as well as average read counts for each genotype and brain region pair may be found in Table S1. Differential expression (DE) analysis was performed for each brain region and age using the DESeq2 v1.20.0[79] package with the Wald test setting. DESeq2's lfcShrink function was utilized to adjust the Log_2Fold Change (LFC) values using the 'normal' shrinkage estimator. Differentially expressed genes (DEGs) were defined as genes with FDR <0.05 and absolute value of LFC >0.2. Bulk RNA-seq DEGs for all ages and brain regions may be found in Table S2. Pearson's correlation r values were calculated using the corresponding LFC values to compare the transcriptomic changes between ages in the same brain region or between different brain regions. Normalized expression values of OXPHOS and ribosomal genes (Figures 2C and 2D; Figures S9B and S9D) were calculated by creating a DESeq2 object from all bulk RNA-seq samples of the thalamus across all ages, running the default DESeq function on this object, then extracting the normalized counts for the genes within 'GO_oxidative_phosphorylation' and 'GO_Ribosome' from the DESeq2 object.

Gene set scoring analysis

To calculate the gene set scores for ARGs, OXPHOS (genes within GO_oxidative_phosphorylation), and synaptic signaling genes (genes within GO_synaptic_signaling), normalized gene expression counts from the bulk RNA-seq analysis as described above was used. First, genes that were not expressed in any samples were filtered out from the normalized counts matrix. Then, to ensure unique gene assignments per gene set, genes appearing in multiple gene sets were removed from the analysis. Using the

moduleEigengenes function from the WGCNA v. 1.73 package,[98] the first principal component of the expression profile of all genes within each gene set in each brain region and animal was computed. This 'module eigengene' was used as a summary measure of each gene set expression. The scores from all brain regions and animals (both genotypes) were pooled by gene set (see Table S9), and pairwise correlations were then assessed across gene sets.

Intron retention analysis

Starting with the FASTQ files, we used a modified version of our previously described in-house pipeline.[99] Reads were mapped to the mm10 genome with STAR v2.7.9a[91] and the command CollectRNASeqMetrics in PICARDTool v2.27.5 (https://broadinstitute.github.io/picard/) was used to calculate QC with the resulting bam. Isoform level quantification was performed with Salmon v1.6.0[90] with -l A –posBias –seqBias –gcBias –validateMapping and a reference based on the GTF and FASTA used for the mm10 10X Cell Ranger reference, with the full genome as decoys. This same reference was used with featureCounts v2.0.1[92] and the BAM produced by STAR to quantify gene expression both with just exonic reads (using the flag "-t exon") and with both exonic and intronic reads (using the flag "-t gene"). Both quantifications were loaded into R v4.0.3 (R Core Team) as data frames. An intronic matrix was generated by subtracting the exonic matrix from the exonic+intronic matrix. Note this is not equal exactly to the number of reads in introns due to ambiguous reads and similar issues. Extensive filtering was performed, removing genes with <101 exonic or intronic reads in total over all samples, whose intronic matrix was negative in any sample, and that had nonzero exonic or intronic expression in less than 2 samples. For each gene we then fit a negative binomial model with the glm_gp command in glmGamPoi v1.4.0,[93] with the formula ~ model (where model is the genotype), with the output the number of reads in the intronic quantification, the offset the log of the number of intronic+exonic reads plus the log of the percent of reads that are intronic, and overdispersion_shrinkage set to True. P-values were then extracted with the test_de command. In thalamus, the regions with highest number of abnormally spliced genes, *Grin2b*$^{+/-C456Y}$ mice exhibited a 1.9% reduction in intronic base content compared to wild types (5.8% (*Grin2b*$^{+/-C456Y}$) vs. 7.7% (wild type), 95% CI: 0.9–2.9%, $p = 0.00676$; linear regression). However, sample to sample variability in % intronic reads may confound this result. A list of abnormally spliced genes, defined as genes with altered % intronic reads with FDR <0.1, in different brain regions of 4-week *Grin2b*$^{+/C456Y}$ mice as well as 4- and 12-week *Grin2a*$^{+/-}$ can be found in Table S5.

TRanscriptome-wide Analysis of Differential Expression (TRADE)

Differential expression effects were re-estimated for each bulk RNA-seq dataset using DESeq2 without LFC shrinkage. R package SVA's[100] num.sv function, run with the be method, was used to determine surrogate variable numbers. TRADE[43] was run on the DESeq2 summary statistics to estimate the distribution of DE effects. The TRADE method generates this estimation by fitting a flexible mixture distribution to the provided gene-wise standard errors and LFC values. Notably, TRADE analysis outputs "transcriptome-wide impact" (TWI) scores, which aims to quantify a perturbation's impact on the transcriptome. We performed permutation analysis to assess the significance of the TRADE estimates. Specifically, we calculated the proportion of TWI estimates that were larger than the empirical estimate across 100 permutations of genotype labels for each dataset. TRADE results for all brain regions, ages and genotypes may be found in Table S3.

Single-nucleus RNA-seq analysis

Single-nucleus RNA-seq (snRNA-seq) reads were aligned to an intron-inclusive mm10 mouse reference genome (https://cf.10xgenomics.com/supp/cell-exp/refdata-gex-mm10-2020-A.tar.gz) using the Cell Ranger v3.0.2 pipeline (10x Genomics).[101] Default parameters were used for running Cell Ranger count, with the addition of the following flags: –chemistry = SC3Pv3 and –expect-cells = 12000. Cell Ranger aggr was run with default parameters to downsample replicates to contain the same number of reads per nucleus in each brain region dataset. Quality control metrics for each sample used in this study may be found in Table S6.

Unique Molecular Identifier (UMI) counts were analyzed using the Seurat v3.2.3[80] package. Nuclei expressing less than 500 genes were removed during preprocessing. The remaining nuclei were normalized by total expression, multiplied by 10,000, and log transformed. Data scaling was then performed using Seurat's ScaleData function. PCA Linear dimension reduction was performed using Seurat's RunPCA function on the scaled data using variable genes, and informative PCs were identified based on an elbow plot generated using Seurat's ElbowPlot function. Seurat's FindNeighbors and FindClusters functions were used to perform clustering on the PCA space. Clusters were then visualized using Uniform Manifold Approximation and Projection (UMAP) on significant PCs. The Scrublet v0.2.3[81] Python package was run with default parameters to identify doublets. Clusters and nuclei with a scrublet score above the region-specific thresholds were determined to be doublets and were removed from the data. The table below shows the scrublet score thresholds for each snRNA-seq dataset.

Dataset	Scrublet Score Threshold
Hippocampus	0.2
PFC	0.4
Striatum	0.4
Thalamus	0.3

Cluster cell type assignment was performed using the Azimuth R package.[82] The reference datasets used for each brain region are summarized in the table below.

Brain region	Azimuth Reference(s) Used
Hippocampus	Allen Brain Atlas "WHOLE CORTEX & HIPPOCAMPUS – 10X GENOMICS",[94] DropViz "annotation.BrainCellAtlas_Saunders_version_2018.04.01.rds"[95]
PFC	Azimuth Mouse Motor Cortex,[96] Allen Brain Atlas "WHOLE CORTEX & HIPPOCAMPUS – 10X GENOMICS"
Striatum	Allen Brain Atlas "WHOLE CORTEX & HIPPOCAMPUS – 10X GENOMICS", DropViz "annotation.BrainCellAtlas_Saunders_version_2018.04.01.rds"
Thalamus	Allen Brain Atlas "WHOLE CORTEX & HIPPOCAMPUS – 10X GENOMICS", DropViz "annotation.BrainCellAtlas_Saunders_version_2018.04.01.rds"

Region-specific cell type marker genes were used to confirm the Azimuth cell type assignments. Similarly, neuronal subtypes were identified by re-clustering nuclei of the given major cell type then marker gene expression was used to confirm the Azimuth subtype identity labels. Widely classified major cell type and subtype marker genes were identified in the literature.[102] Seurat's FindMarkers function was used to identify marker genes for clusters that did not express the common marker genes. These markers were then queried on dropviz.org[95] and/or mouseBrain.org[103] to evaluate the cell type identity. A list of the number of nuclei per cell type per sample can be found in Table S6.

Pseudocell differential expression analysis of snRNA-seq

We employed a pseudocell[53] approach for the snRNA-seq DE analysis, as described in our previous study.[42] Pseudocells were created for the major cell types and subtypes using the.sconline.PseudobulkGeneration function with the following parameter values: pseudocell.size = 40, min_size_limit = 20, nPCs = 30. For the current study, we ran pseudocell generation in randomized mode by setting the rand_pseudobulk_mod parameter to TRUE for pseudocell generation. In this mode, cells are randomly assigned to pseudocells in each cell type from each individual. This is different from non-randomized pseudocell generation, where pseudocells are created by grouping cells into pseudocells based on their similarity in gene expression profile. While randomized pseudocell may not capture topological variation in expression profile within a given cluster to the same extent as non-randomized pseudocell, we opted for using this more conservative setting to reduce the potential of false positives. This effect is especially noticeable when investigating large, heterogeneous cell populations, as non-randomized pseudocell generation may result in pseudocells consisting of specific subtypes or outlier populations. We also noticed that non-randomized pseudocell generation may be impacted by the ordering of cells within the Seurat object, further emphasizing these potential outlier populations. Randomized pseudocell more evenly distributes such populations across pseudocells, reducing the likelihood of identifying subtype marker genes or outlier genes as differentially expressed. We also re-analyzed the single-nucleus RNA-seq data from our previous study using randomized pseudocell.[42] The overall conclusions agreed well between the two analyses.

Cell types and subtypes that were identified but did not have enough nuclei present to create at least two pseudocells per replicate were removed. The clusters that were identified in the initial clustering for each brain region and removed for the pseudocell analysis due to low nuclei counts are as follows: **Hippocampus**: Cajal Retzius, Endothelial, Ependyma, Vascular; **PFC**: Endothelial, Vascular, SST Chodl inhibitory subtype, L6b excitatory subtype; **Striatum**: Ependyma, Vascular; **Thalamus**: Endothelial, Ependyma, Vascular, Fibroblast.

Differential expression analysis was performed using limma's duplicateCorrelation mixed model analysis function with robust empirical Bayes moderated t-statistics and mouse ID as random effect.[104] Genotype and the percentage of mitochondrial reads were used as covariates and orig.ident was used as the random effect for all analyses. Limma's internal background gene identification was used by setting the bkg_genes parameter to NULL. Genes with Benjamini-Hochberg adjusted p-value of less than 0.05, absolute LFC >0.2 and absolute robustness score >0.8 were deemed as DEGs. A list of all DEGs for all cell types and brain regions from pseudocell analysis can be found in Table S7.

Gene set enrichment analysis

The DESeq2 t-stat values from bulk RNA-seq analysis or the LFC values from pseudocell analysis were extracted to run Gene Set Enrichment Analysis (GSEA)[105] using the fGSEA v1.16.0 package[85] and either the C5 v7.2 gene set collection (including 14,765 Gene Ontology (GO) terms) from Molecular Signature Database (http://www.gsea-msigdb.org/gsea/msigdb), or gene sets generated from the literature. Annotations extracted from Ensembl's BioMart data service were used to map mouse gene symbols from the transcriptomics results to *Homo sapiens* homolog-associated gene symbols. GSEA was then performed using the mapped human symbols. Significant GO terms (FDR <0.05) for all tested ages and brain regions may be found in Table S4 for bulk RNA-seq and Table S8 for snRNA-seq analysis.